JV 58 – EFFECTS OF BIOMASS COMBUSTION ON SCR CATALYST

Final Report

Prepared for:

AAD Document Control

U.S. Department of Energy
National Energy Technology Laboratory
PO Box 10940, MS 921-107
Pittsburgh, PA 15236-0940

Cooperative Agreement No. DE-FC26-98FT40321
Performance Monitor: Charles Miller

Prepared by:

Bruce C. Folkedahl
Christopher J. Zygarlicke
Joshua R. Strege
Donald P. McCollor
Jason D. Laumb
Lingbu Kong

Energy & Environmental Research Center
University of North Dakota
15 North 23rd Street, Stop 9018
Grand Forks, ND 58202-9018

2006-EERC-09-03 September 2006

DOE DISCLAIMER

This report was prepared as an account of work sponsored by an agency of the United States Government. Neither the United States Government, nor any agency thereof, nor any of their employees makes any warranty, express or implied, or assumes any legal liability or responsibility for the accuracy, completeness, or usefulness of any information, apparatus, product, or process disclosed or represents that its use would not infringe privately owned rights. Reference herein to any specific commercial product, process, or service by trade name, trademark, manufacturer, or otherwise does not necessarily constitute or imply its endorsement, recommendation, or favoring by the United States Government or any agency thereof. The views and opinions of authors expressed herein do not necessarily state or reflect those of the United States Government or any agency thereof.

EERC DISCLAIMER

LEGAL NOTICE This research report was prepared by the Energy & Environmental Research Center (EERC), an agency of the University of North Dakota, as an account of work sponsored by the U.S. Department of Energy, Montana–Dakota Utilities Co., the Lignite Research Council, the North Dakota Industrial Commission (NDIC), the Electric Power Research Institute, and Xcel Energy. Because of the research nature of the work performed, neither the EERC nor any of its employees makes any warranty, express or implied, or assumes any legal liability or responsibility for the accuracy, completeness, or usefulness of any information, apparatus, product, or process disclosed, or represents that its use would not infringe privately owned rights. Reference herein to any specific commercial product, process, or service by trade name, trademark, manufacturer, or otherwise does not necessarily constitute or imply its endorsement or recommendation by the EERC.

NDIC DISCLAIMER

This report was prepared by the EERC pursuant to an agreement partially funded by NDIC, and neither the EERC nor any of its subcontractors nor NDIC nor any person acting on behalf of either:

(A) Makes any warranty or representation, express or implied, with respect to the accuracy, completeness, or usefulness of the information contained in this report, or that the use of any information, apparatus, method, or process disclosed in this report may not infringe privately owned rights; or

(B) Assumes any liabilities with respect to the use of, or for damages resulting from the use of, any information, apparatus, method, or process disclosed in this report.

Reference herein to any specific commercial product, process, or service by trade name, trademark, manufacturer, or otherwise does not necessarily constitute or imply its endorsement, recommendation, or favoring by NDIC. The views and opinions of authors expressed herein do not necessarily state or reflect those of NDIC.

EFFECTS OF BIOMASS COMBUSTION ON SCR CATALYST

ABSTRACT

A portable slipstream selective catalytic reduction (SCR) reactor was installed at a biomass cofired utility boiler to examine the rates and mechanisms of catalyst deactivation when exposed to biomass combustion products. The catalyst was found to deactivate at a much faster rate than typically found in a coal-fired boiler, although this may have been the result of high ash loading rather than a general property of biomass combustion. Deactivation was mainly the result of alkali and alkaline-earth sulfate formation and growth in catalyst pores, apparently caused by alkaline-earth ash deposition on or near the pore sites. The high proportion of biomass in the fuel contributed to elevated levels of alkali and alkaline-earth material in the ash when compared to coal ash, and these higher levels provided more opportunity for sulfate formation. Based on laboratory tests, neither catalyst material nor ammonia contributed measurably to ash mass gains via sulfation. A model constructed using both field and laboratory data was able to predict catalyst deactivation of catalysts under subbituminous coal firing but performed poorly at predicting catalyst deactivation under cofiring conditions. Because of the typically higher-than-coal levels of alkali and alkaline-earth elements present in biomass fuels that are available for sulfation at typical SCR temperatures, the use of SCR technology and biomass cofiring needs to be carefully evaluated prior to implementation.

TABLE OF CONTENTS

LIST OF FIGURES

Continued…

LIST OF FIGURES, CONTINUED

Continued…

LIST OF FIGURES, CONTINUED

LIST OF TABLES

EFFECTS OF BIOMASS COMBUSTION ON SCR CATALYST

EXECUTIVE SUMMARY

Currently in the United States, coal combustion supplies roughly 2 trillion kWh of electricity annually. Electricity production from biomass combustion is nominally 60 billion kWh, or 3% of total U.S. electrical production. However, the push for greenhouse gas emission reductions is encouraging many in the power industry to consider increased use of biomass in power production. The biomass used for electricity generation absorbs its carbon directly from the atmosphere during its growth, so biomass used for combustion has reduced net carbon emissions as compared with fossil fuels.

Cofiring biomass with coal is an attractive short-term option for reducing CO_2 emissions. Existing coal-fired stations may be able to blend biomass into their coal feed without significant changes in operating conditions or equipment, eliminating the need for construction of new installations to handle 100% biomass feedstocks. In addition to reduced CO_2 emissions, cofiring may also offer benefits in reduced emissions of NO_x and SO_2. Some working experience is available for biomass cofiring. However, little is known of biomass cofiring with low-rank U.S. coals, such as North Dakota lignites and Powder River Basin (PRB) coals. Before biomass can be cofired with these coals on a large scale, several technical issues must first be addressed. One of the issues to be resolved is the effect of biomass cofiring on ash behavior and selective catalytic reduction (SCR) unit performance.

To study SCR catalyst deactivation under biomass cofired ash, a portable slipstream SCR reactor was installed in a utility boiler cofiring 80% biomass with 20% PRB coal. Because of the geometry of the boiler system, ash loading was unusually high at the port used to sample a gas stream for the slipstream reactor, and plugging prevented the reactor from operating continuously for more than a few weeks at a time.

A section of the catalyst was removed after 43 days of operation and replaced with a new section. The new section and the two remaining sections were removed after 171 days of operation, thus providing catalyst sections that had been in place for 43, 128, and 171 days. The sections were analyzed to determine activity coefficients that were then translated into equivalent rates for a full-scale SCR unit. The initial deactivation rate for a full-scale system was predicted to be between 6% and 9% per 1000 hours, which is an order of magnitude greater than the rate reported for SCR units at coal-fired boilers. For the small-scale system used in this study, an inverse rate law for catalyst deactivation was assumed based on theory and known solutions.

The mode of catalyst deactivation was combined alkali and calcium sulfate formation and growth at catalyst pore openings. In previous SCR studies at the EERC, only calcium sulfate was found in the catalyst pores. The difference most likely occurred because more alkali was available in the biomass than in a typical coal, and the initial form of calcium in the biomass fuel readily decomposed to stable calcium carbonate at the low flame temperatures found in this system. Both of these factors are a result of the high proportion of biomass present in the fuel and may not apply to cases with lower biomass-to-coal ratios. Thermodynamic calculations

showed calcium carbonate to be somewhat more stable than calcium sulfate under the conditions found in the SCR, so calcium present as carbonate was not capable of reacting with gas-phase sulfur to form calcium sulfate, leaving only alkali available to undergo sulfation. Ash analysis verified the presence of carbonate in the ash and also showed that little sulfate was present in ash deposited on the catalyst surface, suggesting that the ash did not begin to undergo sulfation until catalyst deposition and was able to form much calcium and alkali sulfate over the catalyst pores.

Thermogravimetric analyzer (TGA) studies of the ash collected upstream of the catalyst revealed that ash sulfation was not measurably affected by the presence of catalyst material or ammonia, either separately or together. TGA work also suggested that sulfation rates were controlled predominantly by the presence of alkali rather than calcium in the ash. These results demonstrate that catalyst deactivation at the utility boiler studied in this work was mainly due to ash deposition and, furthermore, suggest that, in cofired systems with lower ash loading, frequent sootblowing may greatly reduce the rate of catalyst deactivation.

The ash deposition data collected from the utility boiler and the catalyst deactivation rates calculated in the TGA were used to construct a model of SCR catalyst deactivation. Results from a previous study firing PRB coal were also used to test the model under noncofiring conditions. The model predicted catalyst deactivation reasonably well for the PRB coal but did a very poor job at predicting either ash deposition or catalyst deactivation in the cofired system.

Because of the typically higher-than-coal levels of alkali and alkaline-earth elements present in biomass fuels that are available for sulfation at typical SCR temperatures, the use of SCR technology and biomass cofiring needs to be carefully evaluated prior to implementation.

EFFECTS OF BIOMASS COMBUSTION ON SCR CATALYST

1.0 INTRODUCTION

Currently in the United States, coal combustion supplies roughly 2 trillion kWh of electricity annually. Electricity production from biomass combustion is nominally 60 billion kWh, or 3% of total U.S. electrical production (1). However, the push for greenhouse gas emission reductions is encouraging many in the power industry to consider increased use of biomass in power production. The biomass used for electricity generation absorbs its carbon directly from the atmosphere during its growth, so biomass used for combustion has reduced net carbon emissions as compared with fossil fuels.

Cofiring biomass with coal is an attractive short-term option for reducing CO_2 emissions. Existing coal-fired stations may be able to blend biomass into their coal feed without significant changes in operating conditions or equipment, eliminating the need for construction of new installations to handle 100% biomass feedstocks (2). In addition to reduced CO_2 emissions, cofiring may also offer benefits in reduced emissions of NO_x and SO_2 (3). Some working experience is available for biomass cofiring (4–6). However, little is known of biomass cofiring with low-rank U.S. coals, such as North Dakota lignites and Powder River Basin (PRB) coals. Before biomass can be cofired with these coals on a large scale, several technical issues must first be addressed. One of the issues to be resolved is the effect of biomass cofiring on ash behavior and selective catalytic reduction (SCR) unit performance.

SCR technology is the most common back-end technology for reducing NO_x emissions from power stations and typically achieves greater NO_x reduction than other methods (7, 8). For utilities facing severe NO_x reduction requirements, SCR may be the only feasible option. European and Japanese utilities have been installing SCR units to curb their NO_x emissions since the 1980s (9), and at least 75 coal-fired plants in the United States have installed SCR units in direct response to the U.S. Environmental Protection Agency's (EPA's) NO_x Budget Trading Program.

SCR systems may be installed in a number of locations in the flue gas stream depending on catalyst type, but they are most often installed in the high-dust environment before the air preheater, as illustrated in Figure 1. The higher temperatures in this region allow use of more efficient zeolite and vanadium or titanium dioxide catalysts (10). However, this efficiency comes at a cost. Because the flue gas upstream of the air preheater has not yet passed through an electrostatic precipitator (ESP) or baghouse, all of the fly ash must pass through the SCR unit and may blind the catalyst by plugging passages or covering surfaces and, thus, reducing the catalyst's reactive surface area. Blinding of the catalyst reduces the amount of NO_x that can be converted to N_2 and H_2O and also allows ammonia, which is added to the flue gas to react with NO_x, to slip through the catalyst unreacted and escape as a pollutant.

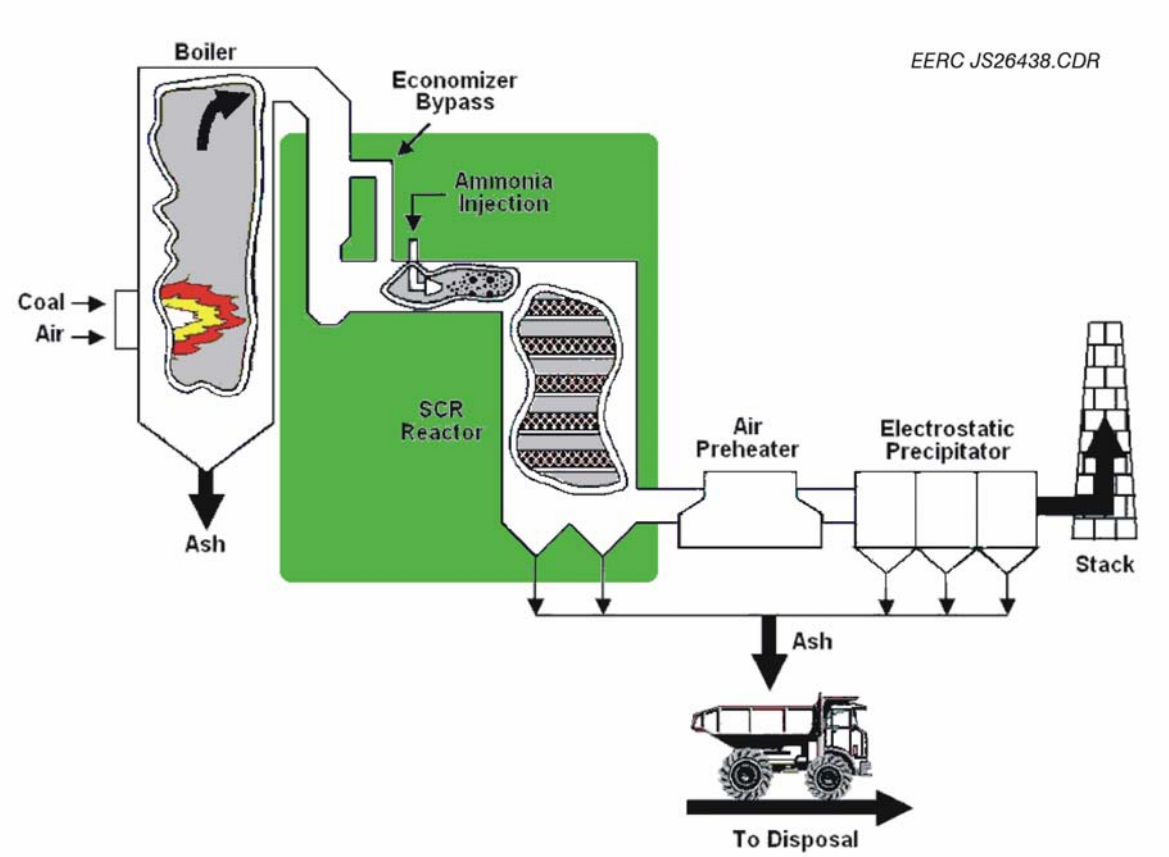

Figure 1. Placement of an SCR reactor in a coal-fired boiler system. Image taken and modified from U.S. Department of Energy National Energy Technology Laboratory (11).

Much research has focused on curbing or better understanding blinding in SCR units installed at coal-burning power stations, but little is known of the effects of biomass combustion on SCR performance. Research on the effects of alkali and alkaline-earth metals on catalyst activity suggests that biomass, which contains high levels of these elements, could be very detrimental to catalyst lifetime when cofired with coal. These elements are likely to form sulfates that deposit on catalyst surfaces and cause blinding or catalyst poisoning (4, 12, 13). In addition to alkali and alkaline-earth metals, phosphorus is also a known SCR catalyst poison found more abundantly in biomass than in coal (5).

As high-dust SCR seems likely to remain the technology of choice for reducing NO_x emissions, SCR catalyst manufacturers must be able to design SCR catalysts that either resist blinding and poisoning from cofired ash or can be cleaned online. The objectives of this study were to provide a greater understanding of how various factors contribute to SCR catalyst deactivation in a cofired power plant and how those factors can be mitigated by examining modes of catalyst deactivation on the bench scale and degree of poisoning and blinding on the full scale.

2.0 BACKGROUND

2.1 Biomass and Greenhouse Gases

One option for reducing net production of CO_2 is to use only biomass as an energy source. Although carbon in the biomass will be released as it is oxidized in flame or in a fuel cell, the following year's crop will remove an equal amount of CO_2 from the atmosphere before being oxidized to extract energy. This cycle of absorbing and releasing equal amounts of carbon has led to biomass being called a CO_2-neutral fuel.

While combustion of 100% biomass may be an attractive long-term option for reducing net CO_2 emissions, most existing power plants in the United States are not designed to handle feeds consisting entirely of biomass. One option for introducing biomass as a fuel source is cofiring biomass with coal. This would allow current power stations to continue operating without significant changes and with reduced net emissions of greenhouse gases.

Much working experience has been gained in biomass cofiring from both the United States and Europe in the last two decades (14). Much of the current knowledge on the problems and solutions to cofiring relates to deposits on boiler tubes, with much less information available for the effect of cofiring on SCR units. This is particularly true for low-rank coals such as North Dakota lignite and PRB coals, which may contain high levels of alkali or alkaline-earth metals, sulfur, and transition metals and can also generate very-fine-particulate fly ash.

Working experience with cofiring has revealed a number of issues that need to be addressed, including SCR catalyst lifetime. Some forms of biomass, such as straw, contain high levels of alkali salts that contribute to fouling in the temperature regime of heat exchange pipes (12). Since most SCR units use mid- to high-temperature catalysts that require installation just downstream of the economizer, alkali sulfates and phosphates may condense on the catalyst surface and reduce catalyst activity. In work performed by Wieck-Hansen and coworkers involving both grate-fired and pneumatically conveyed, wall-fired pulverized coal (pc) boilers cofiring up to 20% straw with coal, a high-temperature catalyst was reported to deactivate at a linear rate of 8% loss every 1000 hours when exposed to high-dust flue gas (4). This rate is significantly higher than the typical catalyst deactivation rate of around 0.7% every 1000 hours for units firing 100% coal (15). While the deactivation rate reported by Wieck-Hansen may have been unusually high owing to factors other than biomass (16), working experience with cofiring other biomass fuels has yielded similar results and has shown alkali and alkaline-earth metals to be associated with rapid catalyst deactivation (6, 17).

Although biomass cofiring can be detrimental to SCR catalyst lifetime, working experience has also shown that cofiring can reduce NO_x emissions at the source (3). Thus, while existing SCR catalysts have the potential to operate less efficiently in cofiring plants than they do in 100% pc-fired plants, the need for NO_x reduction might not be as significant. Moreover, wood-based biomass typically contains less alkali material than straw and less ash than straw or coal, so there is less opportunity for catalyst poisoning and blinding (18, 19). This may make wood cofiring a more attractive option than straw cofiring for reduced NO_x emissions.

2.2 Low-Rank Coals

Low-rank coals such as lignite and PRB coals are common in the upper Midwest and Texas and are burned extensively in these regions as cheap, low-sulfur alternatives to bituminous coal (20, 21). Similar to many biomass fuels, low-rank coals can contain higher alkali and alkaline-earth metal contents than other coals. Additionally, sodium and calcium deposits often form and condense on cool surfaces between the burner and the air preheater. The ash fractions of fine particulate matter that form generally are higher than is common for mid- to high-rank coals (12, 21). These problems cause fouling of boiler tube pipes as well as affect the performance of SCR systems.

3.0 EXPERIMENTAL

An SCR slipstream reactor constructed as part of a previous project was installed in a utility boiler cofiring wood and coal. This reactor is illustrated in Figure 2, in which the direction of flue gas flow should be taken to be top to bottom on the hot (left) side of the furnace wall. This boiler is a stoker-fired unit that burns 80% wood waste with 20% coal. The wood waste is primarily hog fuel (tree bark), with some sawdust. The coal is a mix of three PRB coals, with the approximate compositions of two of these coals given in Table 1. It should be noted that the coal

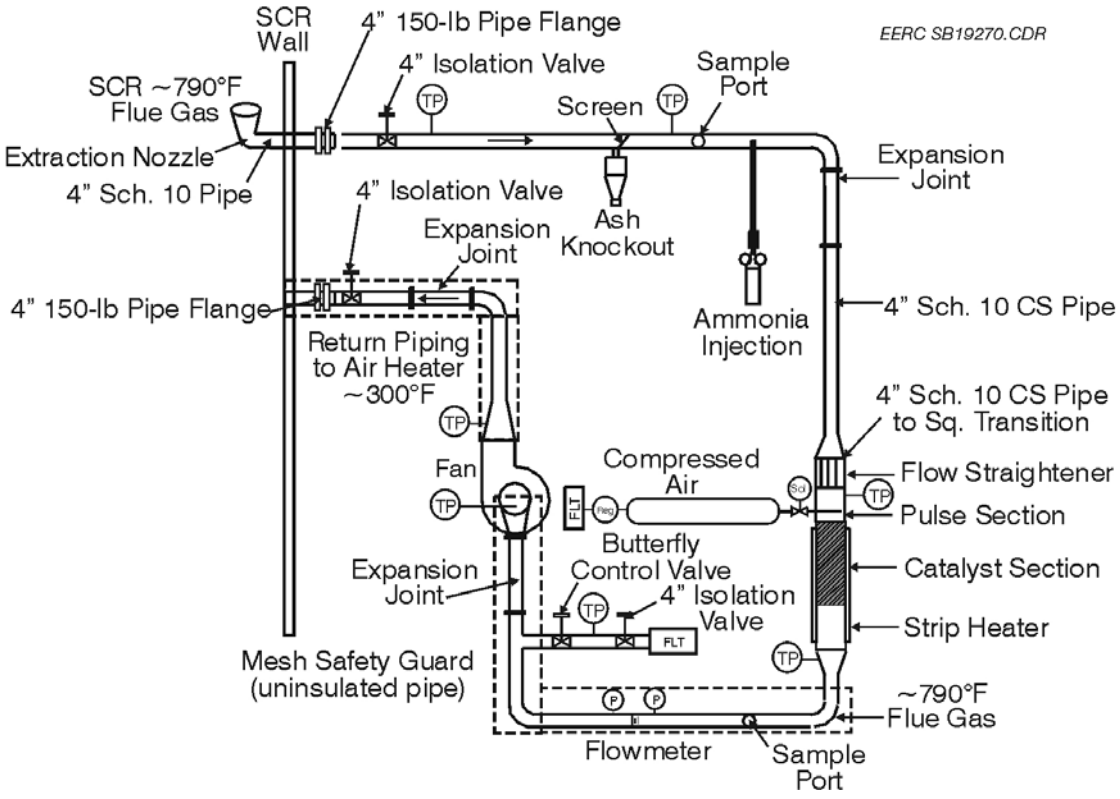

Figure 2. Schematic of the slipstream SCR reactor.

Table 1. Approximate Composition of PRB Fuels Burned at Utility Boiler

	Coal A	Coal B
Prox./Ult. Analysis, wt%		
Moisture	23.60	22.25
Volative Matter	31.74	34.60
Fixed Carbon	38.33	39.42
Ash	6.33	3.73
Hydrogen	6.24	6.45
Carbon	54.02	55.69
Nitrogen	0.75	0.70
Sulfur	0.55	0.34
Oxygen	32.11	33.10
Ash	6.33	3.73
Btu/lb	9439	9791
XRF Ash Analysis, wt%		
SiO_2	40.02	30.65
Al_2O_3	20.21	18.26
Fe_2O_3	1.86	5.47
TiO_2	1.00	1.36
P_2O_5	0.82	0.27
CaO	13.08	16.78
MgO	6.26	6.22
Na_2O	1.02	5.24
K_2O	0.35	0.27
SO_3	15.39	15.52

samples analyzed were not taken from the boiler feed but did originate at the mines that supply the boiler. The fuel is flung onto the back of a conveyer grate and burns as the grate carries it forward. The temperature of the flue gas at the sample location is approximately 800°F. The slipstream reactor is designed to sample the gas stream isokinetically, and the gas cools slightly as it approaches the reactor zone. The reactor zone is held at a constant temperature of 700°F by electric heaters mounted on the outside of the reactor.

The SCR slipstream reactor consists of the control room, the heated reactor section, the fan, and the required piping. The control room is shown in Figures 3–5. The ammonia injection piping is shown on the outside of the control room in Figure 3. For this project, ammonia injection was not used because of safety concerns at the plant. The control room is air-conditioned to cool the electronics, which includes the computer that controls the system and through which remote monitoring was accomplished.

Figure 3. Exterior SCR control room with air conditioner, ammonia injection system, and manual pressure readouts visible.

Figure 4. Interior SCR control room with air conditioner, several control boards, and breaker panel visible.

Figure 5. Exterior control room with interior visible through doorway.

All of the features in the control software could be accessed remotely, allowing the system to be not only monitored but controlled from a remote location via a dial-up modem. Figure 6 shows a screen grab of the control software. On the left side of the screen are displayed key operating parameters, including various temperatures, pressure drops, flow rates, and the fan speed. Beside the temperature window is a button that allows the fan to be turned on or off remotely as well as two toggles for logging data. The button beneath the toggles, labeled "PULSE," is used to manually pulse the catalyst section using bursts of 100-psi air to clear the unit of ash when the pressure drop becomes too high.

Down the center of the screen are graphs displaying the proportional integral derivative (PID) control signal to the fan, the calculated gas face velocity through the reactor in m/s, the volumetric flow rate of flue gas, the pressure drop through the reactor, and the reactor inlet temperature, as listed from top to bottom. On the right side of the screen, the total run time and current time of the day are displayed at the top. Beneath this are sliders and buttons for controlling the fan speed in both manual and PID control modes. In manual mode, the fan speed is set directly; in PID mode, the fan speed is adjusted to maintain a specified gas face velocity through the reactor. The controls beneath the "VFD AUTO" button are normally used for controlling the tempering air (TA) valve; however, hardware problems during the early phases of this experiment made automatic TA control impossible, and the valve was manually adjusted by plant operators for the duration of the test.

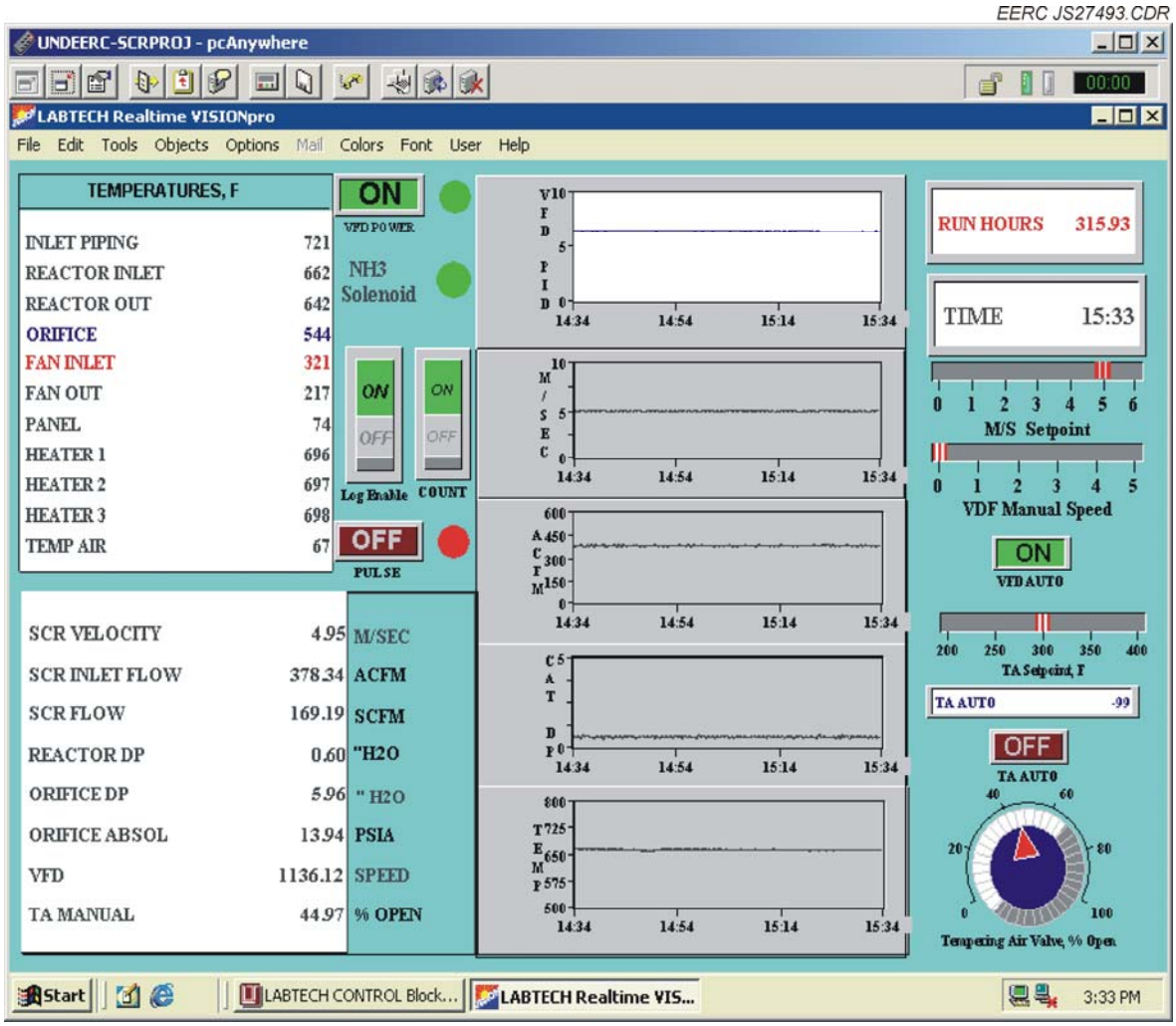

Figure 6. Screenshot of control software for SCR reactor.

Figure 7 shows the fan used to draw the slipstream from the ductwork, with the blue-handled tempering air valve attached to the inlet piping. The induced-draft (ID) fan was sized to pull a pressure of at least 30 in. W.C. It is capable of operating at up to 3600 rpm and 20 hp, with a maximum safe operating temperature somewhat higher than 300°F. During this study, errors with the data interpretation software caused the maximum fan speed to be reported as 900 rpm because speed was reported as ¼ of time speed.

Figures 8–10 show the flow straightener, the flow straightener in the upper reactor chamber, and the reactor chamber, respectively. The reactor chamber illustrates the transition of round to square pipe to accommodate the flow straightener and catalyst. The flow straightener is, just as the name implies, used to reduce turbulence in the gas flow and to attempt to drive any ash particles entrained in the gas straight through the reactor, thus reducing the amount of ash settling onto the catalyst.

Figure 7. ID fan and TA control valve.

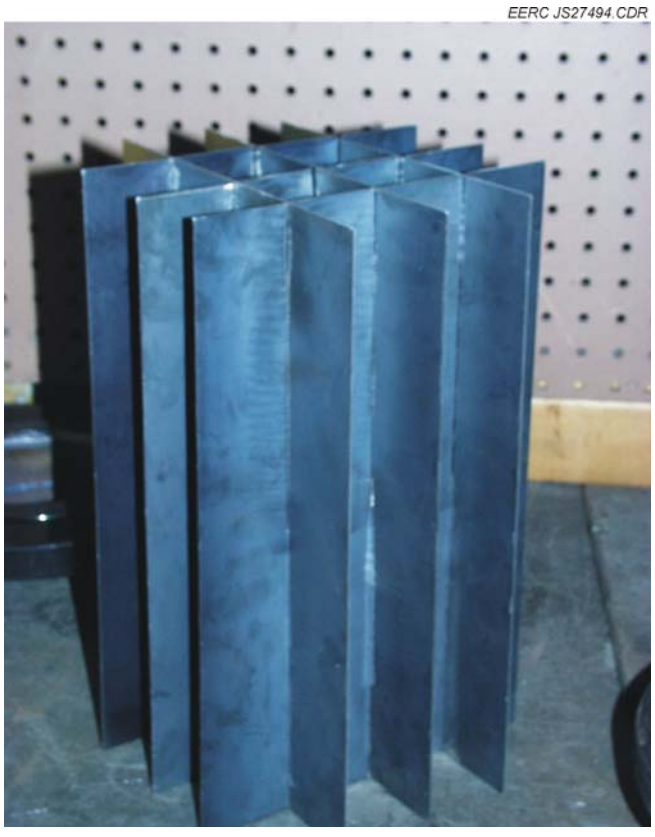

Figure 8. Flow straightener used to reduce turbulence in the reactor.

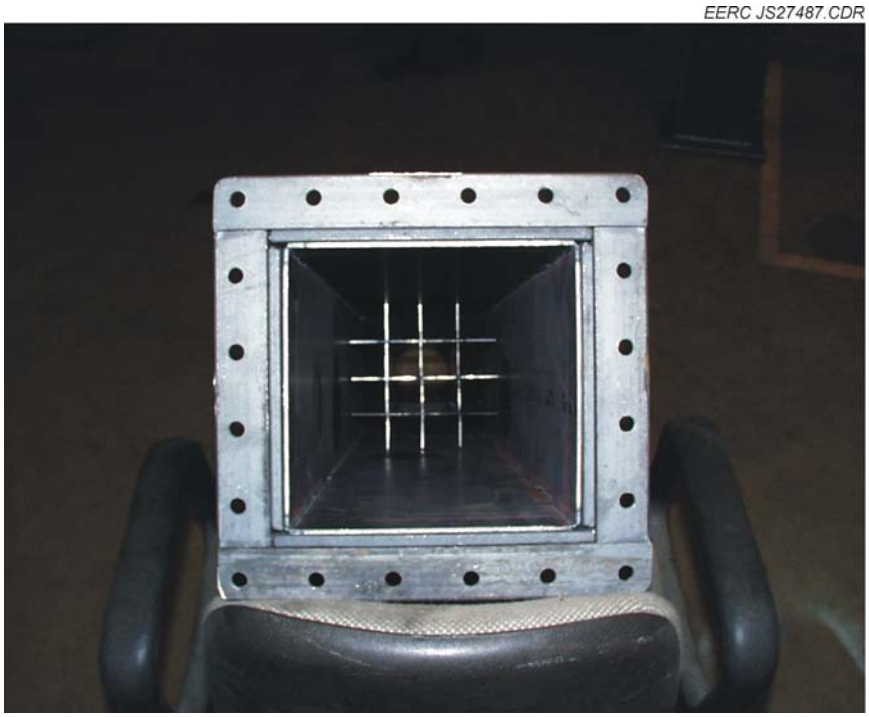

Figure 9. Flow straightener inside of reactor chamber.

Figure 10. Reactor chamber.

Figure 11 shows the new catalyst sections in the lower half of the reactor chamber prior to start-up. Figure 12 shows the reactor being installed at the test site. The control room is to the left side of the image, and the rectangular section in the center of the image is the heated reactor portion of the system. The flow direction is downward through the heated section. The gas path then is briefly turned horizontal before being turned vertical to go up to the next floor, as seen in the right of Figure 12. On the next floor up, the gas is drawn through the ID fan and sent back into the duct work of the boiler. Although insulation is seen covering the horizontal and vertical sections of piping in Figure 12, this was later removed to help cool the gas to a temperature within the fan's safety limits.

A section of catalyst was removed from the SCR reactor after 43 days of operation. A segment of this catalyst was cut and placed into the holder shown in Figure 13, which was then connected to gas inlet and outlet tubes and placed inside of a bench-scale furnace. Simulated flue gas with the composition given in Table 2 was passed over the catalyst at 14 L/m and 650°F, and NO_x concentrations were measured in the gas outlet stream to determine NO_x conversion efficiency. Tests were done with low-NO_x concentrations (125 ppm) and also with high-NO_x concentrations (600 ppm) to determine whether catalyst activity was a function of NO_x concentration. The same method was also used on a segment of fresh catalyst to establish baseline catalyst efficiency.

Ash samples were collected from the horizontal piping leading to the SCR reactor, from the top surface of the catalyst, and from the elbow below the SCR reactor where the piping turns 90° to pass through an orifice plate flowmeter. All three ash samples were analyzed by x-ray fluorescence (XRF), computer-controlled scanning electron microscopy (CCSEM), and carbon–

Figure 11. Clean, new SCR catalyst sections inside reactor chamber.

Figure 12. Installation of reactor chamber at test site with control room, reactor chamber, and piping visible.

Figure 13. Catalyst holder for bench-scale testing. The rectangular section is approximately 14 inches long.

Table 2. Simulated Flue Gas Concentration During Bench-Scale Tests of SCR Catalyst

	Concentration	
Species	First Test	Second Test
O_2	6%	6%
CO_2	12%	12%
H_2O	15%	15%
SO_2	600 ppm	600 ppm
SO_3	12 ppm	12 ppm
NO	120 ppm	600 ppm
NO_2	6 ppm	6 ppm
NH_3	50–150 ppm	600 ppm
Hg	12 μg/m^3	12 μg/m^3
HCl	1 ppm	1 ppm
N_2	Balance	Balance

hydrogen–nitrogen (CHN) analysis to determine composition. The ash samples from the horizontal piping and the elbow beneath the catalyst were also analyzed qualitatively for the presence of known crystal phases by x-ray diffraction (XRD).

CCSEM is a technique using automated scanning electron microscopy (SEM) to locate and measure the size of inorganic particles ranging from 1 to 300 μm in coal and other fuels. Energy-dispersive x-ray spectroscopy (EDS) is used in conjunction with the imaging process to determine the composition of the mineral fractions of the ash. The chemical composition is then fed to a computer program that determines mineralogy of the detected particles. This process is useful in determining relationships between particle size and mineralogy and is detailed elsewhere (22, 23).

CHN analyses were performed by combusting samples at 900°C in 100% oxygen to convert all carbon, hydrogen, and nitrogen to CO_2, H_2O, and N_2. The product gas was split into three equal portions. Each portion of gas was scrubbed to remove all components except one, and the remaining component was then passed over a thermal conductivity detector (TCD) to determine the amount present. The results were calibrated using a standard, and software calculated the percent of each element present in the original sample.

Samples of the ash from the horizontal piping and from the top surface of the catalyst were mixed with ground catalyst in a 1:1 ratio and placed in a DuPont 951 thermogravimetric analyzer (TGA). The catalyst used for this TGA work was scraped from the support substrate of an unused catalyst section. The TGA consists of a sensitive electronic scale in a sealed tube. Gas passes through the tube at a set temperature or heating/cooling rate and may react with samples on the scale, leading to mass gains or losses that are recorded at defined intervals. This allows estimation of absorption/desorption rates from the weighed sample and can also be used to study oxidation and decomposition.

The mixed ash–catalyst samples were heated under N_2 to 600°, 700°, and 800°F in the TGA. Once the desired temperature was reached, simulated flue gas consisting of 14% CO_2, 8% H_2O, 4% O_2, 400 ppm SO_2, 100 ppm NH_3, and the balance N_2 was passed over the samples for 2 hours as sample weight was recorded at 6-second intervals. Fresh catalyst was also tested in the TGA to establish a baseline weight gain.

After the TGA tests, the samples containing ash collected from the horizontal piping in the SCR were analyzed under an SEM at 200× magnification to determine composition. Untested samples of ash and catalyst were also analyzed to determine what gas species had reacted with the ash and catalyst material. Thermodynamic modeling was performed using the Facility for the Analysis of Chemical Thermodynamics (FACT) software to verify that the apparent species were likely to form under the conditions in the TGA. This software predicts molar fractions of stable gas-, solid-, and solid solution (i.e., mineral)-phase components in a system by minimizing the total Gibbs' free energy.

TGA results and data from previous SCR slipstream tests were used to construct a computer model. This model was designed to predict both catalyst deactivation with time and ash loading on the SCR surface. Ash loading determined what fraction of the SCR cross section was unblocked from gas flow and able to react. The product of catalyst surface activity and fractional cross-sectional area determined the effective overall catalyst activity.

4.0 RESULTS AND DISCUSSION

4.1 Operating Conditions

When the SCR reactor was first installed, ash would build up rapidly and cause the reactor to plug completely, often within a day of start-up as seen in Figure 14. To limit the amount of ash entering the system, the inlet pipe was turned from a vertical, isokinetic sampling position 45° to the flow of the gas stream. When this proved insufficient to limit ash intake, the inlet piping was turned to a 90° angle, and then, finally, to a 180° angle. In this position, the pipe entrance pointed away from the entering gas stream, meaning that the ID fan had to draw flue gas into the system against the normal direction of flow. Because of this, the fan ran under higher capacity than was observed in previous work using this slipstream reactor. Reactor shutdowns were more frequent than in previous tests as the fan lacked the extra capacity to adjust for process upsets, thus limiting the amount of gas available to the system.

The SCR operated under conditions of relative normalcy (non-zero-gas velocity, reactor temperature near 700°F, sufficient run time to achieve near-steady state) for a total of 171 days. These 171 days were not consecutive, as unexpected upsets in both the SCR reactor and the boilers at the power station forced the SCR unit to be shut down irregularly. In general, when the reactor was shut down, it would be cleaned of ash before being restarted.

The total time that the reactor was in place at the plant spanned 20 months, from May 2004 to January 2006. Data collected during this period are provided below in Figures 15 and 16, with key events numbered and explained briefly in Table 3 and more thoroughly in the following text.

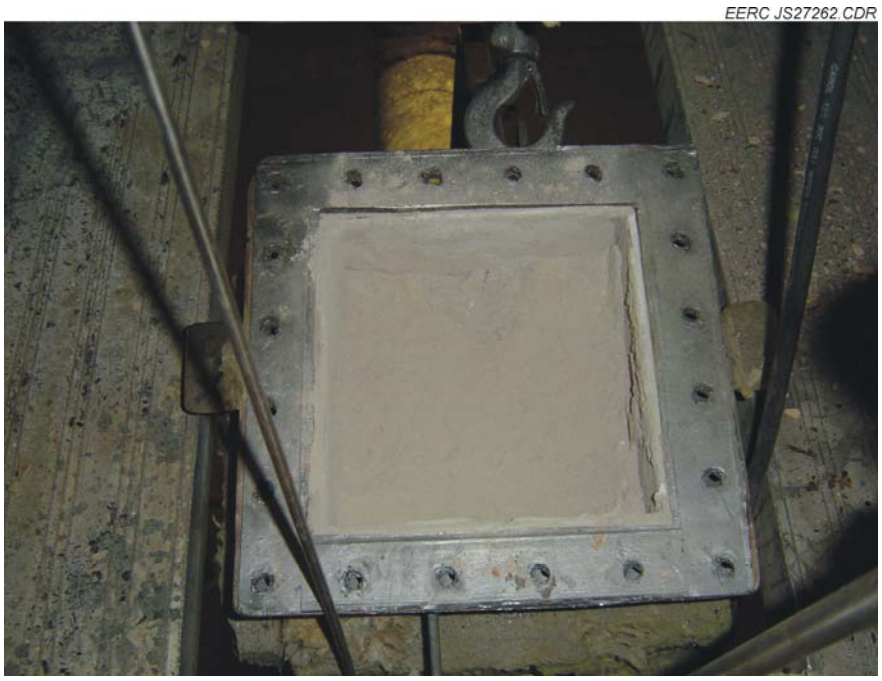

Figure 14. Ash completely plugging catalyst channels to cause 100% reduction in gas flow.

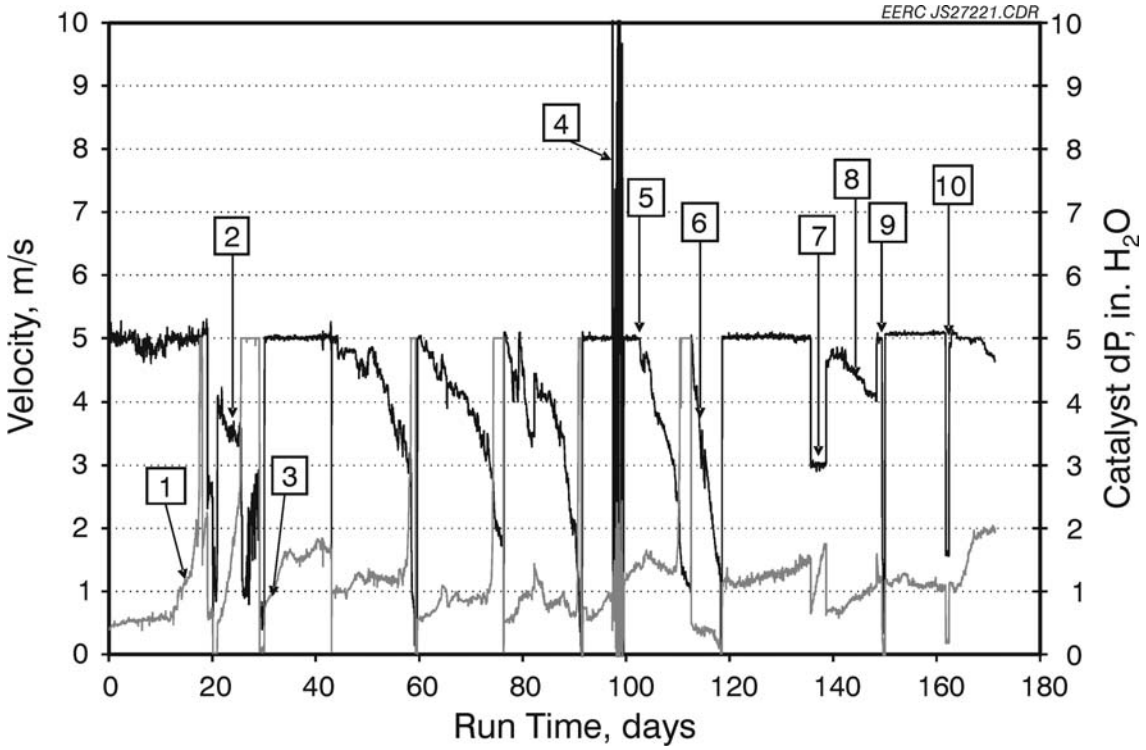

Figure 15. SCR velocity and pressure drop across SCR catalyst during operation. Data in black represent velocity, and data in gray represent catalyst dP.

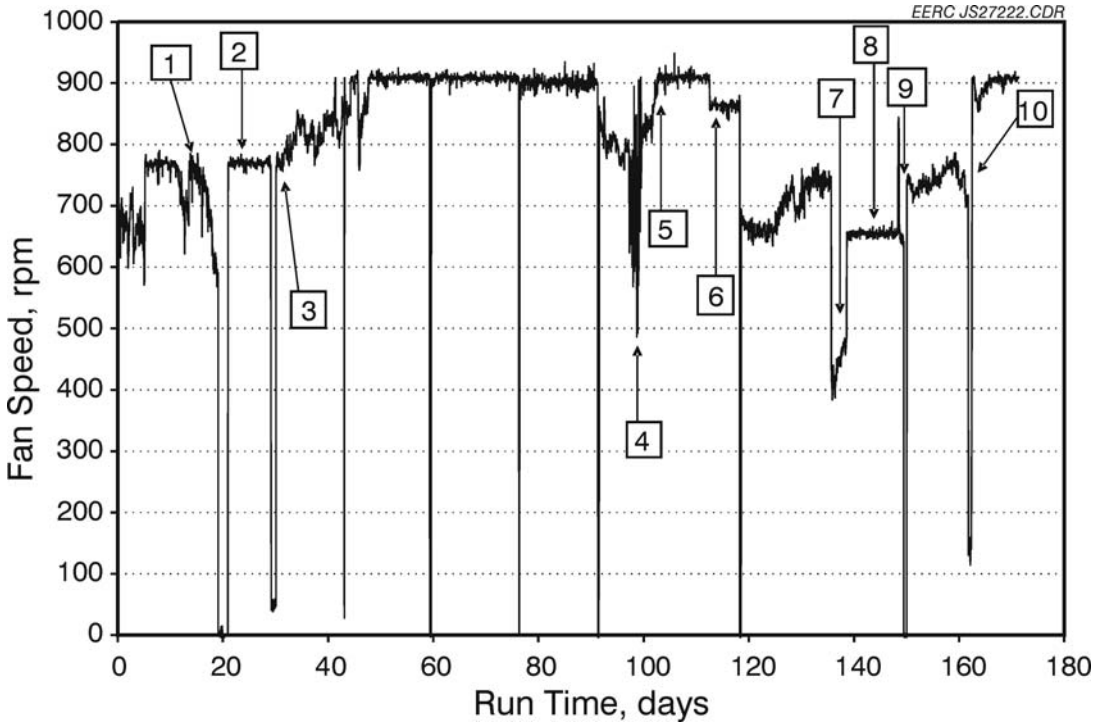

Figure 16. ID fan rotation speed during SCR operation.

Table 3. Key Events Enumerated in Figures 15 and 16

Event	Description
1	One of the orifice pressure taps apparently plugged, resulting in calculation of a higher-than-actual SCR velocity.
2	The PID control failed to maintain SCR velocity.
3	The SCR sootblower pulse rate was switched to once every 2 minutes.
4	The orifice thermocouple broke, making calculation of the SCR velocity impossible.
5	The SCR began to plug severely over Labor Day weekend when no one was around to notice.
6	The PID control failed to maintain SCR velocity.
7	The ID fan inlet temperature rose too high on a Friday afternoon when no engineer was at the plant to check the tempering air valve, so the SCR velocity set point was dropped to 3.0 m/s to achieve sufficient fan cooling until Monday morning.
8	The PID control failed to maintain SCR velocity.
9	The PID started to work again.
10	The ID fan inlet temperature rose too high during Christmas break when no one was at the plant to check the tempering air valve, so the SCR velocity set point was dropped to 1.5 m/s to achieve sufficient fan cooling.

Table 4 provides overall average values for key variables as well as a breakdown of average values during each segment of continuous operation.

Figure 15 illustrates a repeating trend that occurred each time the SCR became plugged with ash. First the catalyst differential pressure would rise to a fairly constant value somewhere between 1 and 2 in. H_2O. The SCR velocity would then slowly drop to nearly zero gas flow, at which point the catalyst differential pressure would rapidly increase to its maximum measurable value of 5 in. H_2O. This implies a highly nonlinear relationship between gas flow and pressure drop. Gas flow through the catalyst could drop considerably without greatly affecting the catalyst differential pressure until all gas flow had been nearly cut off, at which point the fan began to pull a significantly stronger vacuum on the downstream side of the catalyst relative to the upstream side.

Another interesting note is that between Days 43 and 91, the fan was continuously running at maximum speed. This was the result of significant ash buildup upstream and downstream of the reactor. Although the catalyst was cleaned during each shutdown, the piping was not cleaned during this period and the reactor would achieve the desired face velocity of 5 m/s only when it was first started. After all ash was removed from the inlet and outlet piping, the reactor was able to maintain face velocity for longer periods of time because the fan was not starting up at full capacity. This long, continuous period of low SCR velocity may have impacted the rate of catalyst deactivation, although whether the net impact would be positive or negative is difficult to say based on the limited data at hand.

Table 4. Durations and Average Run Time Values of Each Continuous Segment of Operation

Dates		Duration,	Total Time,	Average Properties		
				SCR Velocity,	Catalyst dP,	Fan Speed,
From	To	days	days	m/s	in. H_2O	rpm
10/1/04	10/19/04	18	18	4.95	0.87	722
1/4/05	1/6/05	2	20	3.85	1.30	301
1/26/05	2/5/05	10	30	2.48	2.44	633
2/9/05	2/22/05	13	43	4.98	1.46	812
3/15/05	3/31/05	17	60	4.04	1.41	878
4/19/05	5/6/05	17	76	3.86	1.35	907
5/25/05	6/9/05	15	91	3.60	1.00	896
8/16/05	9/6/05	21	113	4.07	1.53	839
10/4/05	10/10/05	6	119	2.76	0.40	823
10/11/05	10/31/05	20	139	4.71	1.26	661
12/2/05	12/13/05	11	150	4.33	0.84	623
12/15/05	1/5/06	21	171	4.87	1.30	790
Overall		171.35		4.22	1.28	780

The first event described in Table 3 is a plugged orifice pressure tap. This likely resulted in an artificially high pressure drop through the orifice. Because SCR face velocity was calculated from the temperature and pressure drop of gas passing through the orifice, the plugged tap would have caused SCR face velocity to appear higher than it actually was. The fan slowed in response to this rise in SCR face velocity, apparently augmenting the problem and causing the fan speed to drop more until it had finally stopped running and the SCR velocity also dropped. Although this makes it impossible to know the true SCR face velocity between Days 14 and 19, the gas temperature at the SCR outlet had a nearly linear relationship with the gas velocity. Since this temperature was dropping while the fan speed dropped but did not drop completely to room temperature, it is safe to assume that the gas velocity was greater than zero but lower than 5 m/s.

Events 2, 6, and 8 all relate to failed PID operation. When the SCR unit was started up, the computer would be used to control the fan speed until the SCR velocity approached 5.0 m/s. PID control would then be used to adjust fan speed to control SCR face velocity. In each of these cases, the PID controller initially stabilized the SCR face velocity at 5.0 m/s, but then the computer would cease to maintain gas velocity. This caused SCR face velocity to drop as ash built up and the fan failed to respond to the resulting drop in gas flow. Event 9 marks one case in which the PID was brought back online without shutting down the SCR. It should be noted that the SCR unit ran nearly without interruption from this point until it was removed.

Event 3 marks the point at which the SCR sootblower pulse rate was increased from once every 30 minutes to once every 2 minutes. This was intended to slow the rate of ash deposition on the catalyst surface and allow for longer periods of continuous operation, but as seen in Figure 17, the pulse rate had little effect on the rate of increase in catalyst differential pressure under normal operation. In fact, the rate rose very rapidly after the pulse rate was increased on Day 30 and did not level off again until Day 35, and this change in rate of differential pressure increase may have been the result of alterations in fuel content and not of any changes in SCR operation. It should be noted that the data in Figure 17 represent Days 2–6 and Days 120–124 in Figures 15 and 16, which were two periods of relatively steady-state operation. In each case, the first day of operation is ignored to provide time for the system to reach steady state. Days 2–6 have a lower average catalyst DP than do Days 120–124 because the catalyst was just installed at this point and there was less restriction through the catalyst.

Event 4 represents a broken orifice thermocouple. Because the algorithm for determining SCR velocity was based in part on assumptions about gas density in the orifice, which were, in turn, based on flue gas temperature, the erratic data provided by this broken thermocouple resulted in erratic results for SCR face velocity. The PID responded to this by rapidly cycling the fan in response to each sudden and random change in calculated gas velocity.

Events 5, 7, and 10 all describe events that occurred either during or just before holidays, vacations, and weekends. Event 5 was the normal effect of ash limiting gas flow through the SCR and occurred at other times but would normally have resulted in an unscheduled SCR shutdown before the SCR face velocity reached as low a level as it did in this case. Events 7 and 10 are the result of user intervention. In both of these cases, the tempering air valve, which was used to provide some cooling air to the fan inlet, became pulled shut and caused the fan inlet

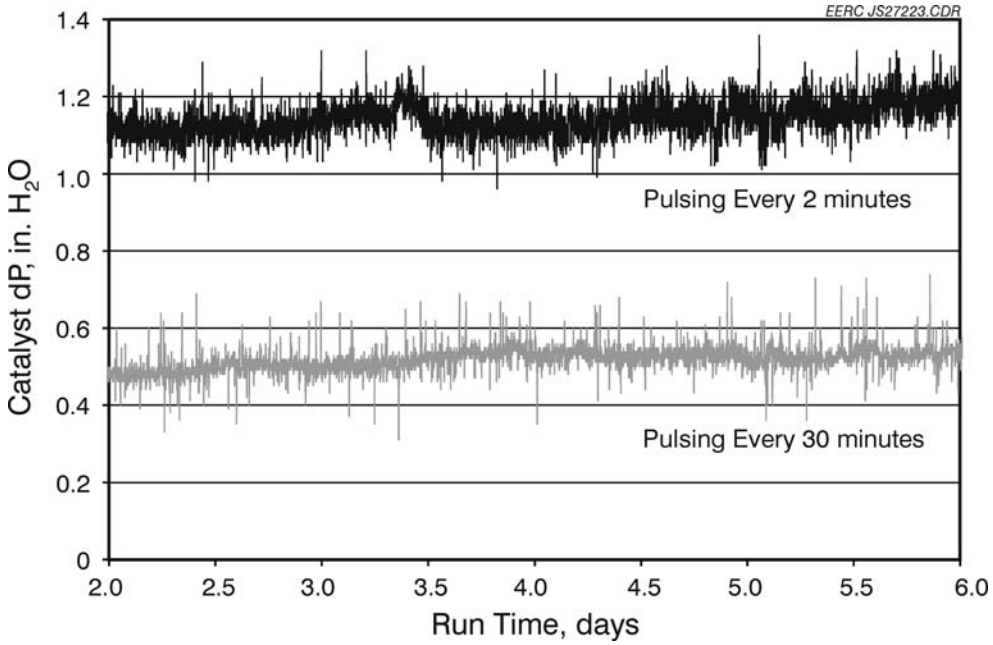

Figure 17. Effect of sootblower pulse rate on pressure drop across SCR catalyst. Data in gray are from October 2–6, 2004, and data in black are from October 12–16, 2005.

temperature to rise to unacceptably high levels. This happened at other times but did not generally result in any process upsets because an engineer was always available at the power station to reopen the valve. However, since Events 7 and 10 occurred during a weekend and holiday, respectively, the set point to the PID was changed to a lower value to limit gas flow and allow the fan to cool until an engineer was back on duty. It should be noted that the controlled shutdown at 150 hours was also in response to a stuck tempering air valve; in this case, the fan inlet temperature was extremely high and the unit was completely shut down to avoid damaging the fan.

These specific events and the generally erratic behavior of the data demonstrate that the SCR reactor was not generally running under optimum conditions. This may have negatively impacted the results such that the reported rate and mode of catalyst degradation are not indicative of typical SCR behavior in a cofired power plant. At the same time, some of these issues also illustrate the difficulty of successfully maintaining a steady-state retrofit SCR reactor in a high-ash cofired power plant.

4.2 Catalyst Deactivation

The catalyst section that was taken from the slipstream reactor after 43 days of operation achieved 75% NO_x removal efficiency both with 126 ppm NO_x and with 600 ppm NO_x. In both tests, NH_3 was initially introduced to the system at concentrations below those required for stoichiometric reaction with NO_x, and its flow rate was then increased until further increases did not result in higher NO_x removal efficiencies. Figure 18 plots NO_x concentration with time for the 43-day catalyst section.

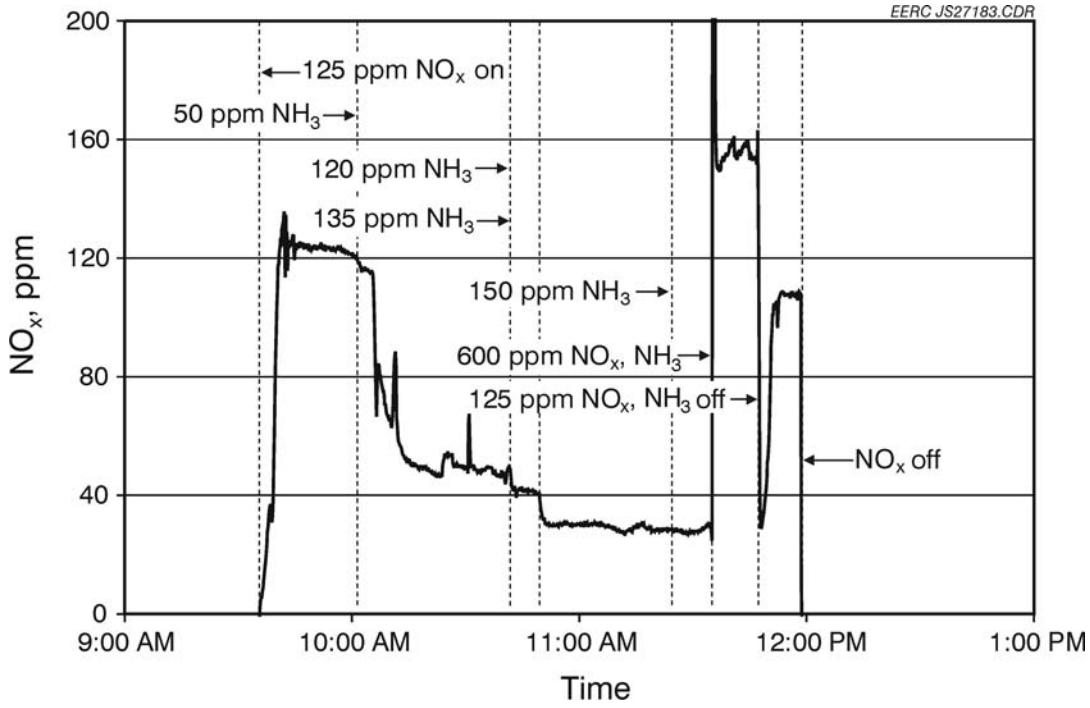

Figure 18. NO_x levels with time in bench-scale furnace test for SCR catalyst section after 43 days of operation.

The catalyst section that was tested as received removed 91% of the NO_x from the simulated flue gas. Since catalyst activity is generally defined as the ratio of reaction rate to initial reaction rate (24), the 43-day SCR catalyst had an activity of 0.82. This represents an average deactivation rate of 18% every 1000 hours, which is significantly higher than the average deactivation rate of 0.7% every 1000 hours for SCR catalysts exposed to coal combustion flue gas (15). Some of this high deactivation rate could be explained if one assumes that the catalyst section continued to deactivate even when not in operation, which is a very unlikely scenario but could be used to provide a lower limit for catalyst deactivation. Since the catalyst section was physically in place for a total of 144 days, the minimum deactivation rate is 5.2%/1000 hours, which is still quite high.

Other investigators have shown that ash concentrations and catalyst deactivation rates may be 2–3 times higher at the inlet than at the outlet of an SCR reactor (4). Since full-scale catalyst sections may be several feet in length, with multiple sections stacked one above the other and the bench-scale reactor is only 14 in. long, the catalyst section tested in this work represents deactivation rate at the inlet of a full-scale unit. Using the rule that deactivation rates are 2–3 times higher at the reactor inlet, catalyst sections in a power plant operating under conditions similar to those at the power plant used for sampling in this study can be expected to deactivate at about 6%–9% every 1000 hours. Again using the very unlikely assumption that the catalyst continuously deactivated even when not at temperature or exposed to flue gas, the absolute minimum deactivation rate for a full-scale SCR system is 1.7%–2.6% every 1000 hours, which is still higher than what is observed for coal-fired plants.

The mode of deactivation in this case appears to be alkali and calcium sulfate formation over catalyst pores, as shown in Figure 19. The alkali and calcium sulfate in this image appear as small spindles pointing down into the pores at the catalyst surface. This pore blocking is likely initiated by deposition of sodium, potassium, and calcium-rich particles on the catalyst surface followed by sulfation and expansion, a mechanism similar to one that has been reported elsewhere (25, 26). Known solutions to models for pore blocking via sintering suggest a deactivation rate that is inverse with respect to time (24). Assuming that the equation describing deactivation takes the form of $a = 1/(1+k_d \cdot t)$, where a is activity, k_d is the rate constant, and t is time, then k_d may be calculated as $k_d = 2.2\times10^{-4}$ h^{-1}, and the full equation for catalyst deactivation becomes:

$$a = \frac{1}{1+\left(2.2\times10^{-4}\,\mathrm{h}^{-1}\right)\cdot t} \qquad \text{[Eq. 1]}$$

Alkali sulfate formation is inferred from TGA results (described later in this paper) and from analysis of alkali and sulfur in the catalyst itself. In both cases, total alkali and sulfur correlate strongly, and the ratio of sulfur to alkali is very nearly identical in both cases, implying that the same compounds (presumably alkali sulfates) had formed. However, analysis of the pore-blocking material did not reveal any strong correlation between sulfur and any other material or combination of materials, although either calcium or alkali was consistently present with the sulfur. The ratio of sulfur to alkali and calcium was generally somewhat lower than it was in either the TGA ash or the catalyst material. This implies that the material in the pores had not completely sulfated. It may be that other compounds (e.g., carbonates, oxides, hydroxides) were also present but could not be detected in the sintered material over the pores because of the

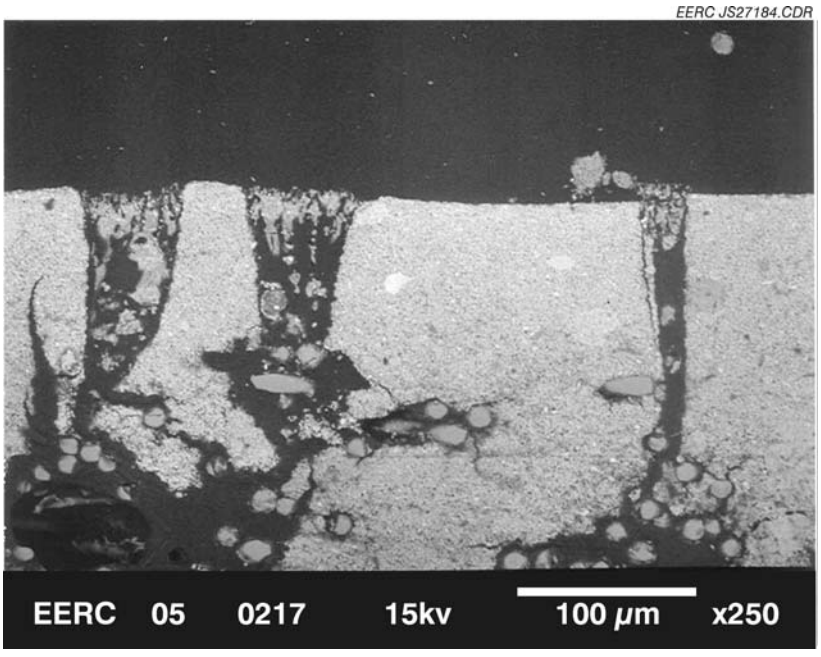

Figure 19. SEM image of blocked catalyst pores after 43 days of operation.

methods used to analyze them. For instance, the sample was mounted in a carbon-based epoxy, so carbon content was uncertain and the presence of carbonates could not be ascertained; likewise, oxygen was detected but could not be attributed to oxides rather than carbonates, sulfates, or other oxygen-containing anions.

As described in Section 4.3, only minor calcium sulfate ($CaSO_4$) was detected in the ash scraped from the top of the catalyst or at the catalyst surface, and the correlation between calcium and sulfur in the ash generally was very poor. By contrast, total alkali and sulfur contents correlated very strongly even within the catalyst, as seen in Figure 20. This implies that sodium and potassium sulfate formation were significant sources of pore closure. This is in disagreement with other researchers, who have reported that calcium sulfation alone dominates as sulfation is promoted by SO_3 formation directly at the catalyst active sites (26). This is also in disagreement with the results of the field testing performed in this study which showed calcium sulfate as a major component of catalyst deactivation as the result of pore blockage, as shown in Figure 19.

An interesting discovery of the SEM examination was the presence of both sulfur and alkali material deep inside the catalyst and at the same ratio observed on the surface. This trend was observed to a depth of nearly 1000 µm (1 mm), as seen in Figure 21. Since fresh commercial SCR catalysts are reported to be doped with up to 1 wt% sulfate for enhancing NO_x reduction

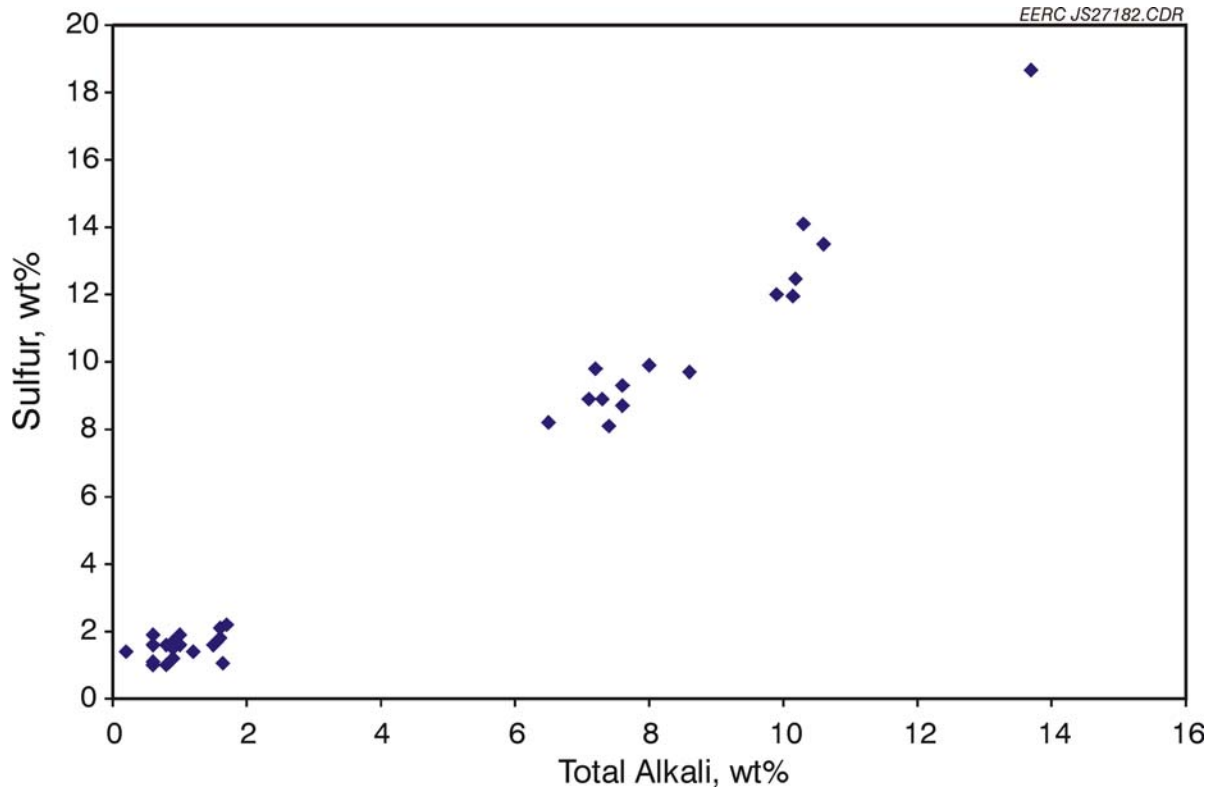

Figure 20. Sulfur correlation with total alkali (Na + K) content on surface and deep inside SCR catalyst.

(27), it may be that data points with alkali sulfate contents of 2% or less represent unpoisoned catalyst material. The sulfur penetration depth would then be reduced from 1000 to 160 µm, which is still fairly deep. Other workers have reported that the entire catalyst volume is effective at promoting SO_2 oxidation, and that sulfur oxidation is dependent on the presence of existing sulfate anions, implying that SO_2 diffuses rapidly through catalyst pores and that sulfate forms throughout the SCR pore structure at reaction temperature (27). The presence of alkali sulfate deep within the solid catalyst bed bolsters the claim of high SO_2 diffusivity in SCR pores.

After one catalyst section had been removed and replaced, no further sections were removed until the end of the test. This represented 171 days (about 6 months) of operation under acceptable conditions for the two original catalyst sections and 128 days for the section that had been installed to replace the first section removed. Activity was calculated by comparing the NO_x removal efficiency of these sections with the efficiency of a fresh catalyst section (which, by definition, had an activity coefficient of 1). The results are plotted in Figure 22.

Oddly, the catalyst section that had been placed in the unit after 43 days of operation suffered the greatest deactivation. This may have been the result of ash build-up in the other catalyst sections forcing more gas flow into the new catalyst section. Comparing the catalyst section in Figure 23 with those in Figure 11, it is apparent that the sections became plugged by large ash particles during the early weeks of the study. Because the reactor setup at the plant had been altered to minimize entrainment of large ash particles in the gas flow entering the SCR, the new catalyst section may never have reached the same degree of internal plugging as the other two catalyst sections and would have continued to see the bulk of the gas flow during the entire

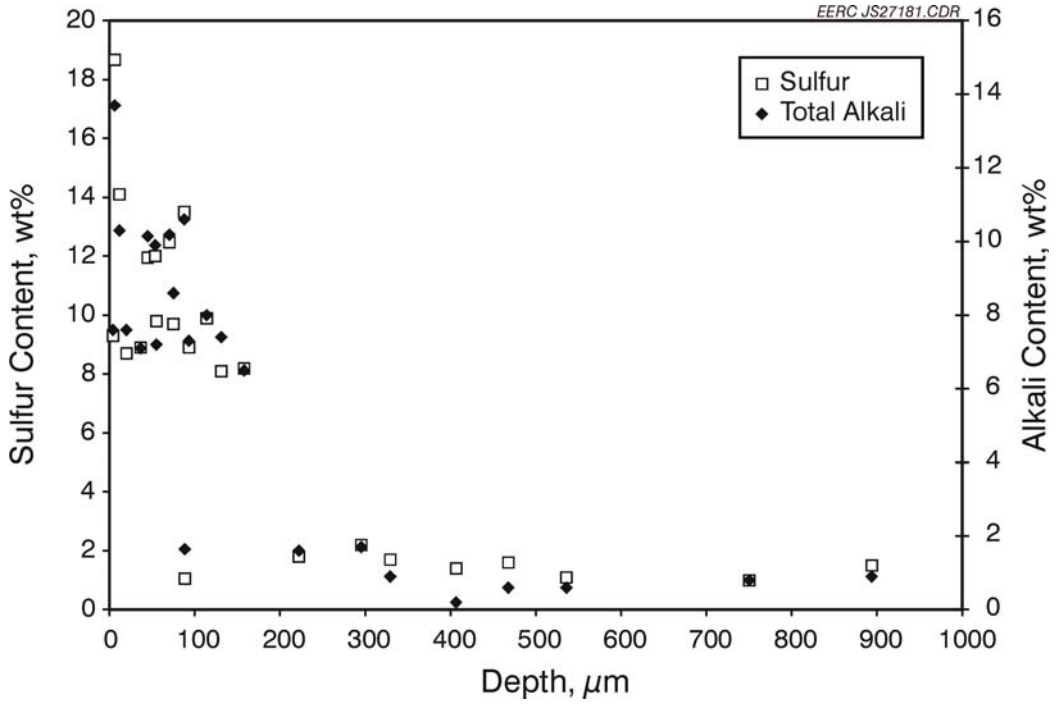

Figure 21. Total alkali (Na + K) and sulfur content with depth beneath catalyst surface.

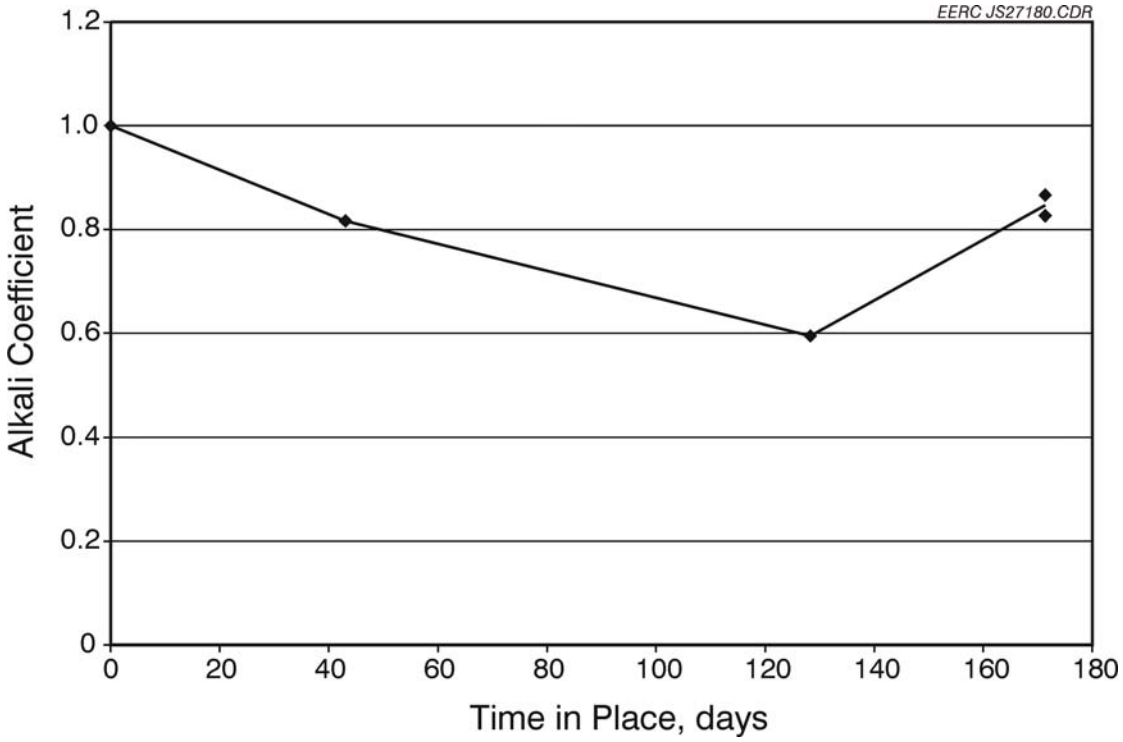

Figure 22. Bench-scale test results of catalyst deactivation with time.

Figure 23. Catalyst section removed after 43 days of operation.

128 days it was in place. This theory is supported by the fact that there is no statistical difference in activity coefficients between the section removed after 43 days and the sections removed after 171 days, implying that the sections left in the reactor for 171 days saw negligible gas flow during the last 128 days of operation. Visual observation of the reactor sections during each shutdown revealed light coming through the channels, so the older sections were not entirely blocked off, but they may have had large ash particles built up inside their channels that caused them to plug more rapidly than the fresh catalyst section. Again, the fresh section would never have seen large ash particles and may have presented the lowest resistance to gas flow even after several cycles of plugging and cleaning.

Assuming the two data points at 171 days of operation represent only 43 days of deactivation, then they may be ignored. The data point at 128 days had an activity coefficient of 0.59. Using the deactivation rate equation provided in Equation 1, the activity would be estimated as $a = 1/[1+(2.2\times10^{-4})(3079)] = 1/1.68 = 0.60$. This is in good agreement with the actual deactivation after 128 days and further supports the claim of an approximately inverse deactivation rate.

4.3 Ash Deposit Chemistry

CHN analyses (Table 5) revealed that the ash sample from the horizontal piping contained 3.8% carbon and that the ashes scraped from the top of the catalyst and collected from the elbow contained 5.2% and 1.6% carbon by weight, respectively. These results were surprising, as the scraped and elbow ashes, seen in Figure 24, appeared blacker than the grayish-tan ash from the horizontal pipe and were expected to contain more unburned carbon. CCSEM analyses (Table 6) showed that the ash from the horizontal piping contained 33% calcite (calcium carbonate, $CaCO_3$) by weight, while the other ashes contained less than half as much of this mineral. Thus most of the carbon found in the piping ash was likely carbonate (CO_3^{2-}) rather than unburned carbon.

Although the CCSEM analysis of the horizontal piping ash showed only 2.9% $CaSO_4$ in the form of gypsum, XRD analysis revealed that the anhydrite form of $CaSO_4$ was a major phase, as seen in Table 8. Some portion of the unknown and calcium-rich fraction in the CCSEM is likely accounted for by the presence of this sulfate material. XRF results support this finding, as 12% of the horizontal piping ash was present as sulfate (Table 7). Converting the values in Table 7 to account for individual elements (rather than oxides) and renormalizing to account for the presence of unknowns (22%, not listed), sulfur accounts for 4.8% of the total sample weight

Table 5. CHN Analyses of Ash Samples from SCR Unit (all compositions are reported as weight percents and are rounded to two significant figures or one decimal place)

Element	Source of Ash		
	Horizontal Piping	Top of Catalyst	Elbow
Carbon	3.8	5.2	1.6
Hydrogen	0.26	0.14	0.07
Nitrogen	0	0.01	0

Figure 24. Ash containing black particles from top of SCR catalyst chamber.

Table 6. CCSEM Analyses of Ash Samples from SCR Unit (all compositions are reported as weight percents)

	Source of Ash		
Mineral	Horizontal Piping	Top of Catalyst	Elbow
Quartz	5.6	23.5	20.1
Iron Oxide	0.3	0.9	1.9
Rutile	0.1	0.0	0.4
Calcite	33.2	13.9	9.0
Dolomite	4.0	3.0	1.1
Ankerite	0.3	0.2	0.4
Kaolinite	0.3	1.5	0.6
Montmorillonite	0.0	0.3	0.0
K Al-Silicate	0.9	4.4	3.9
Ca Al-Silicate	0.8	0.9	0.7
Na Al-Silicate	0.1	0.3	0.6
Mixed Al-Silicate	0.8	1.4	7.1
Fe Silicate	0.0	0.0	0.1
Ca Silicate	2.5	5.0	6.8
Ca Aluminate	0.2	0.1	0.4
Gypsum	2.9	0.5	0.2
Apatite	0.1	0.0	0.0
Gypsum/Al-Silicate	0.2	0.0	0.3
Si-Rich	0.8	2.1	1.4
Ca-Rich	13.2	5.0	4.5
Ca-Si-Rich	0.7	0.4	4.5
Unclassified	32.8	36.3	35.9

Table 7. XRF Analyses of Ash Samples from SCR Unit (all compositions are reported as normalized weight percents and are rounded to two significant figures or one decimal place)

	Source of Ash		
Oxide	Horizontal Piping	Top of Catalyst	Elbow
SiO_2	10	47	50
Al_2O_3	4.3	11	10
Fe_2O_3	1.3	3.8	5.1
TiO_2	0.3	0.4	0.5
P_2O_5	1.6	1.3	1.1
CaO	57	25	21
MgO	4.1	2.7	2.3
Na_2O	4.5	3.5	3.7
K_2O	4.9	3.5	3.4
SO_3	12	2.3	2.8

Table 8. Qualitative XRD Analysis of Ash Samples

	Nominal	Major/Minor Presence	
Major Phases	Compositions	Horizontal Piping	Elbow
Calcite	$CaCO_3$	Major	–
Portlandite	$Ca(OH)_2$	Major	–
Anhydrite	$CaSO_4$	Major	Minor
Periclase	MgO	Minor	–
Quartz	SiO_2	Minor	Major
Gehlenite	$Ca_2Al_2SiO_7$	Minor	–
Anorthite	$CaAl_2Si_2O_8$	Minor	Major
Lime	CaO	Minor	–
Hematite	Fe_2O_3	–	Minor
Brownmillerite	$Ca_2(Al,Fe)_2O_5$	Possible	–

if all species are assumed to be fully oxidized, as they are in Table 7. Thermodynamic modeling, which is discussed later in this paper, predicted that the ash would form approximately 20%–25% $CaSO_4$ at equilibrium. This amount of sulfate would provide 4.7% sulfur by weight, which is close to the calculated value of 4.8% and suggests that significant calcium sulfate was present in the collected ash material.

The large fraction of calcite in the ash from the horizontal piping is a result of calcium oxalate in the hog fuel. The white spots seen in Figure 25 represent calcium oxalate phytoliths in a piece of wood. Calcium oxalate decomposes in three steps, first losing water at about 120°C, then CO to form calcium carbonate at 500°C, and finally losing CO_2 to form calcium oxide at 625°C (28). In the system from which this ash was taken, small fuel particles such as sawdust are present in the fuel as it is flung over the conveyer grate to the rear of the boiler. When this

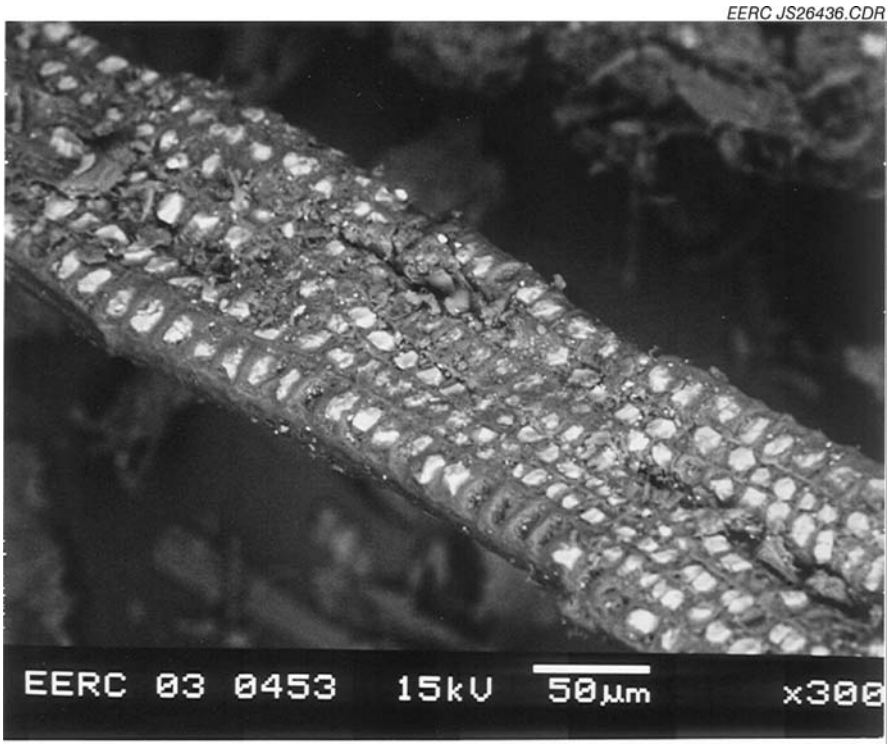

Figure 25. SEM image of hog fuel showing high calcium-oxalate content of fuel.

occurs, it is likely that much of the smaller, lighter fuel particles are entrained in the flue gas and carried out of the furnace without ever seeing the hot part of the flame. As a result of these lower combustion temperatures, oxalate in the fuel may not have completely decomposed to reactive oxide. Moreover, the gas temperature at the ash collection point and in the SCR was below 800°F (427°C), so the gas was not hot enough to decompose calcium carbonate into calcium oxide after deposition. This likely accounts for the large calcite peaks seen in the ash XRD.

As seen in Figure 26, the lower combustion temperature also resulted in the formation of numerous irregular and rhomboidal ash particles in addition to the spherical fly ash that typically results from high-temperature pulverized coal combustion.

The ashes from the SCR and from the elbow both contained over 20% quartz as compared to 5.6% quartz in the horizontal piping ash, as shown in Table 6. They also contained higher fractions of silicates, aluminosilicates, and silicon-rich material, and the two major phases detected in the XRD were quartz and anorthite, a calcium-rich aluminosilicate. These indicate the presence of feldspars or phytolith-derived material in the ash. This also helps to explain why very little sulfate was present in the ash samples from the top of the SCR catalyst or from the elbow below the catalyst relative to the ash from the horizontal piping, since less calcium was available to form sulfate.

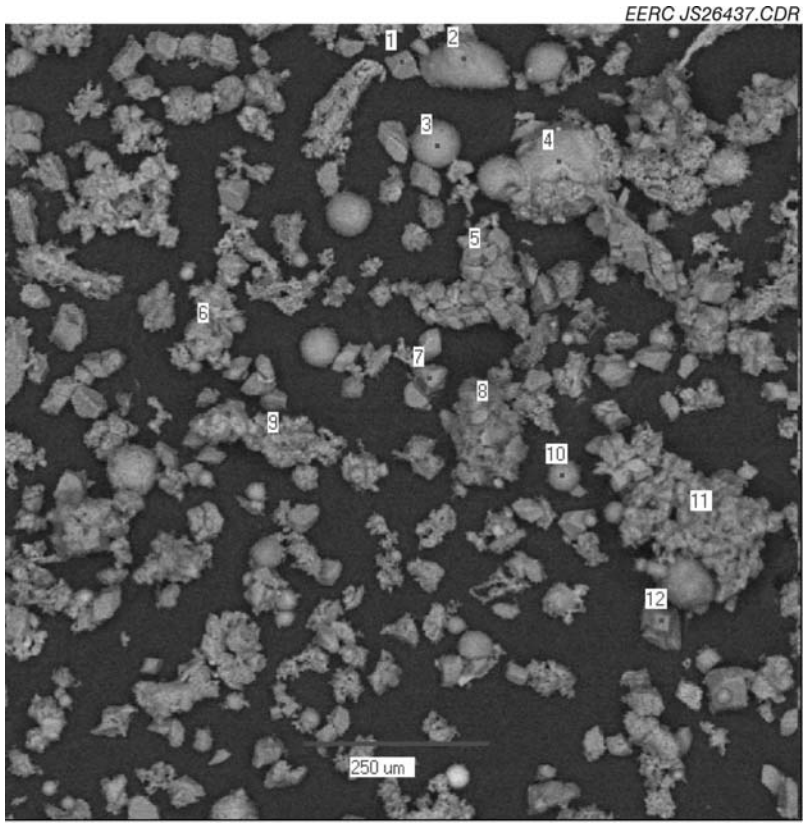

Figure 26. SEM image of ash particles from horizontal piping in slipstream SCR.

Previous studies on low-temperature deposition for high-calcium, low-sulfur coals showed that calcium does not undergo sulfation until after deposition (29). This trend is apparent in the ash collected from the surface of the SCR reactor and likely contributed to high deactivation rates. Comparison of thermodynamic modeling results and ash composition shows that the ash collected from the top of the reactor contained significantly less sulfur (0.92%) than would be expected at equilibrium (2.4%), demonstrating that the ash had not fully sulfated. The presence of alkali and alkaline-earth metals in a state capable of undergoing further reaction with gas-phase sulfur may have contributed to catalyst deactivation by sulfate growth over catalyst pores.

CCSEM analysis revealed that the ash particles from the SCR and the elbow were, on average, significantly larger than the ash particles from the horizontal pipe: Almost all of the SCR and elbow ash was classified as 46–100-µm-diameter particulate matter, while over 50% of the ash particles from the pipe were less than 22 µm in diameter, as seen in Figure 27. The likely reason for this difference in particle sizes is that large particles, which have high momentum, impacted on the catalyst surface as a result of sudden changes in gas flow direction on entering the honeycomb catalyst channels. Likewise, large particles would have collected at the elbow because it is actually a tee with the bottom capped off and is designed to capture large ash particles. Contrarily, particle deposition in the horizontal piping would have been less selective toward large particles.

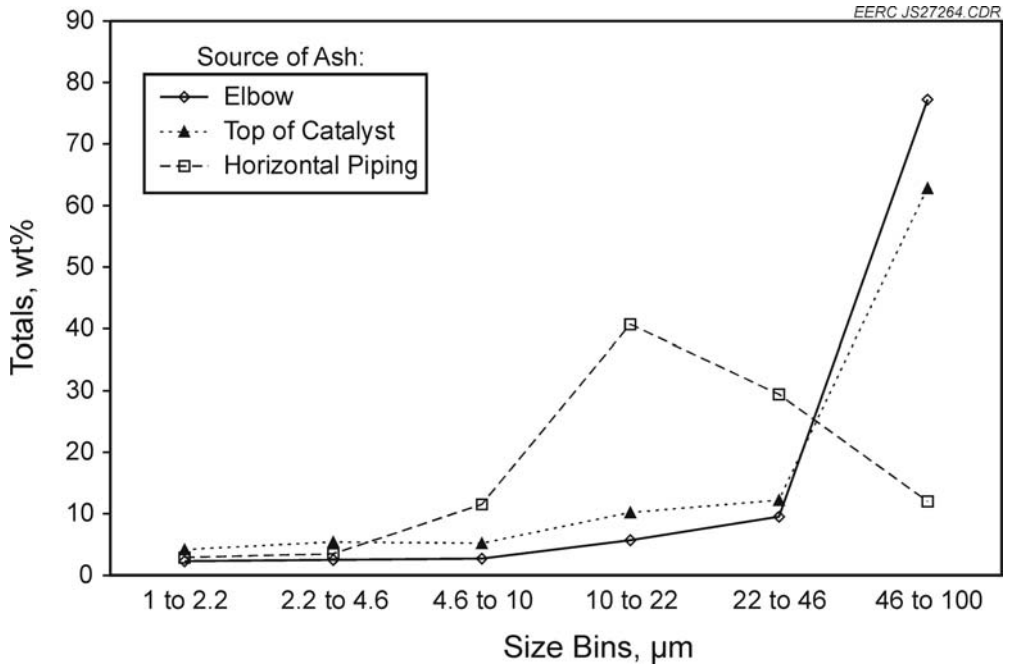

Figure 27. Size fractionation for ash particles collected from various locations in SCR slipstream reactor.

CCSEM analysis of mineral phase by particle size revealed that the size bins for calcite were in the 10–22-µm range for all three ash samples in Figure 27. By contrast, other mineral phases exhibited different size fractionations for each ash sample. Because calcite is thought to have formed from the uniformly–sized calcium oxalate phytoliths seen in Figure 25, which appear to be in the size range of 10–22 µm, it is reasonable that most calcite particles would form at the same size. Thus the high calcite fraction found in the ash from the horizontal piping is probably the result of more small particles depositing in this section of the reactor than in other sections.

4.4 TGA Results

Figure 28 plots weight gain with time as measured in the TGA for the SCR catalyst material only. Figure 29 plots weight gain with time for SCR catalyst mixed with ash taken from the horizontal piping leading into the SCR reactor, and Figure 30 plots the same for SCR catalyst mixed with loose ash collected from the top of the catalyst. As seen in Figure 28, the pure catalyst is most prone to mass gain at 600°F and showed no detectable mass gain at 800°F.

As seen in Figures 29 and 30, the rate of mass gain tends to increase with increasing temperature for the mixed ash–catalyst samples and gives consistent results with repeat tests. Moreover, the change in rate of mass gain increases with temperature, so that increasing the temperature from 700° to 800°F results in a larger rate increase than does increasing the temperature from 600° to 700°F. This suggests a mass gain rate that may be exponential with temperature, which, in turn, implies mass gain due to chemical reaction in accordance with the Arrhenius equation.

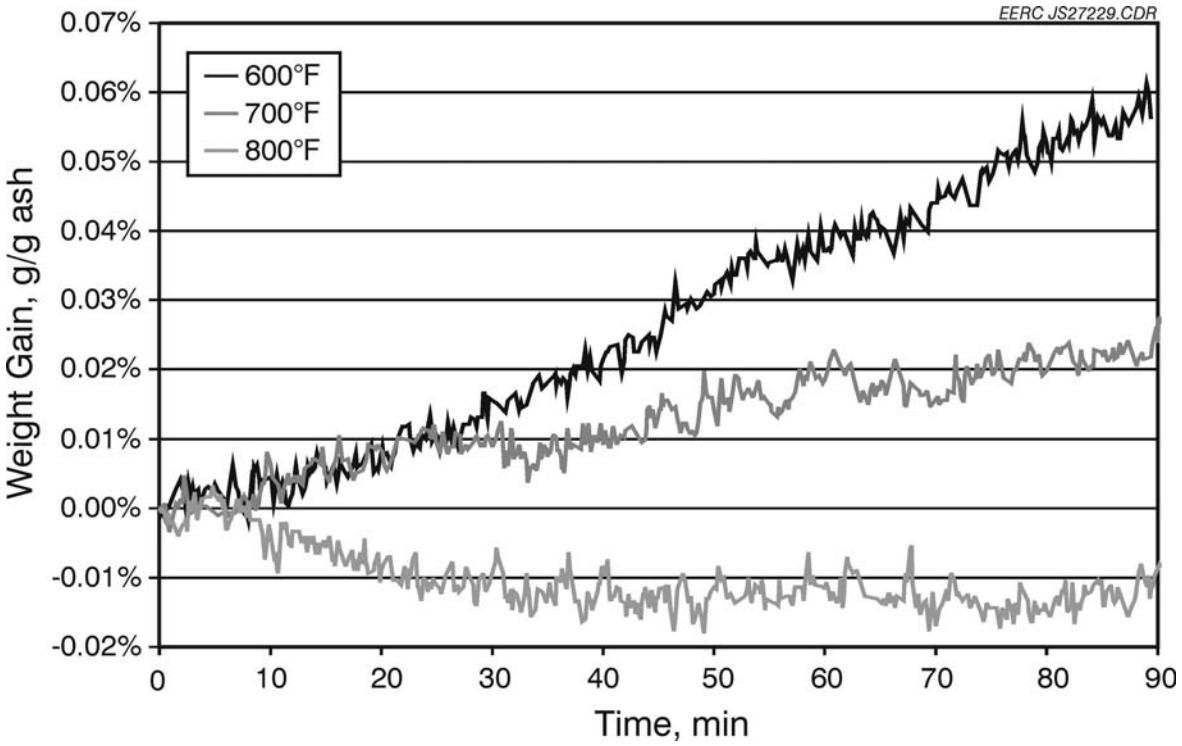

Figure 28. Weight gains with time for 100% SCR catalyst under simulated flue gas.

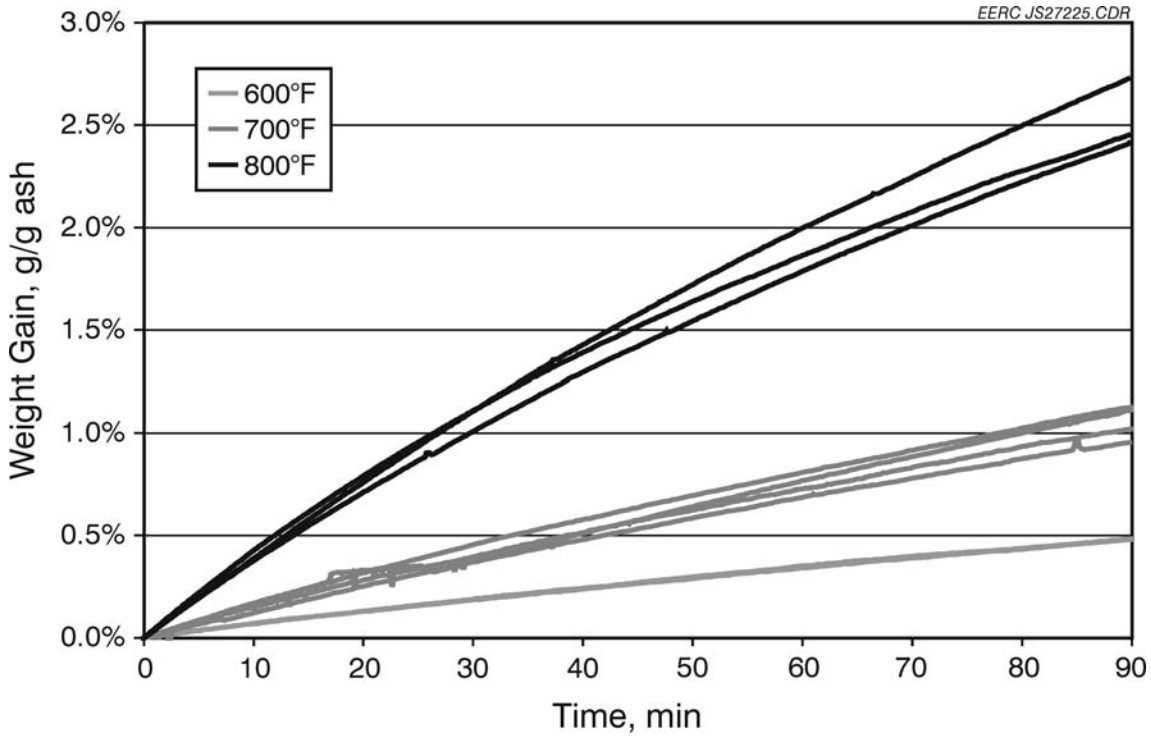

Figure 29. Weight gains with time for 1:1 horizontal piping ash–SCR catalyst mixture under simulated flue gas.

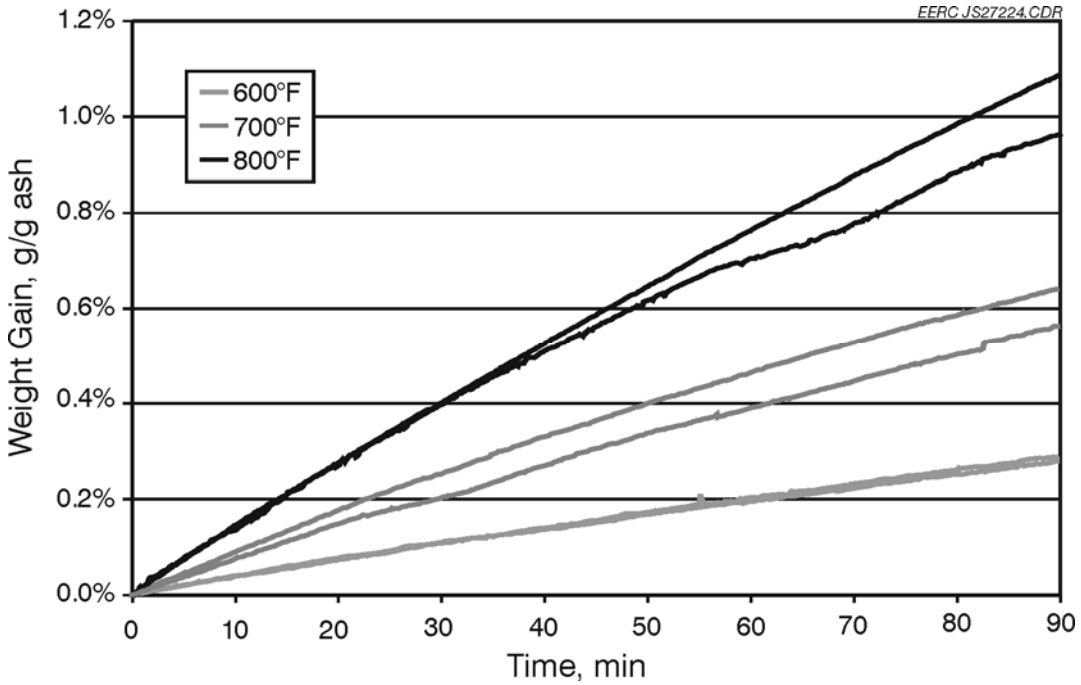

Figure 30. Weight gains with time for 1:1 scraped ash–SCR catalyst mixture under simulated flue gas.

The weight gains in Figure 30 are significantly lower than the weight gains in Figure 29. This is likely the result of lower alkali and alkaline-earth metal content, as shown in Table 7.

Figure 31 shows mass gain for ash samples without catalyst. These tests (and the tests with catalyst) were performed at several gas velocities to ensure that sufficient gas flow was passing through the TGA. Surprisingly, the presence of catalyst does not appear to have contributed to mass gain, as mass gains were reduced by half when half of the ash was replaced by catalyst. Previous studies have shown that mixed ash and catalyst tend to undergo sulfation much more rapidly in a TGA than does either catalyst or ash alone (25). The only major difference between this TGA work and the previous work (aside from the type of ash) is that NH_3 was injected into the TGA in this test but not in the previous work. Since NH_3 is known to almost completely inhibit sulfur oxidation over SCR catalyst at levels as low as 100 ppm (27), it was thought that the ammonia might have indirectly inhibited sulfation by preventing SO_2 from oxidizing to form reactive SO_3. However, repeat TGA tests performed without NH_3 showed no change in the results, as shown in Figures 32 and 33. It may be that the catalyst used in this test is simply more selective than the catalyst materials used in previous tests and, as a result, it does not cause significant sulfation outside of catalyst pores.

Point morphologies taken in the SEM revealed a correlation between alkali material and sulfur content in ash particles, as seen in Figure 34. Ignoring three apparent outliers, the molar ratio of sulfur to alkali is 1.71. This trend was observed in ash that had been through the TGA tests but was not apparent in the untested ash. This implies that the mass gain observed in the TGA was the result of gas-phase SO_2 and ash alkali material reacting to form alkali sulfates. This

is in agreement with the SEM results from the slipstream reactor shown in Figure 20, in which the ratio of alkali to sulfur was 1.76. Thermodynamic modeling also supports the claim of alkali sulfate formation, as alkali sulfates were predicted to constitute greater than 6% by weight of the reaction products between gas and ash at equilibrium over the range of temperatures at which the TGA tests occurred. Figure 35 presents the predicted ash content of select species at equilibrium.

No correlation was observed between sulfur and alkaline-earth metals in post-TGA ash. In a similar study done on PRB coals, low-sulfur U.S. bituminous coals, and lignite, sulfur was reported to increase with calcium, implying that calcium sulfate was the major reaction product in the TGA (25). The coal ashes used in the previous study contained less sodium and potassium than the ash used in this work, and none of the ash material that was analyzed by CCSEM contained significant levels of calcium carbonate. While thermodynamic modeling predicted that the ash used in the current investigation would form 20% calcium sulfate or more at equilibrium, as shown in Figure 35, XRD results (Table 8) revealed that calcium in the horizontal piping ash may have already reached an equilibrium level of sulfation. Moreover, most of the remaining calcium in the ash was present as stable calcium carbonate, which was a result of calcium oxalate in the fuel. Since calcium oxalate and calcium carbonate are not nearly as reactive as is calcium oxide, they would not have a strong tendency to sequester sulfur from the gas phase.

Figure 36 presents average EDS analyses of all ash particles examined in the SEM from before and after the TGA tests. All results are normalized to 100% closure with the elements shown. Sulfur content increased with TGA temperature, suggesting that alkali sulfate formation occurs most rapidly at higher temperatures. This is in agreement with the weight gains shown in Figures 29 and 30. Average sulfur appears to be higher in the as-received ash than in the ash after the 600° or 700°F TGA tests; however, this is due to two erratic data points in the

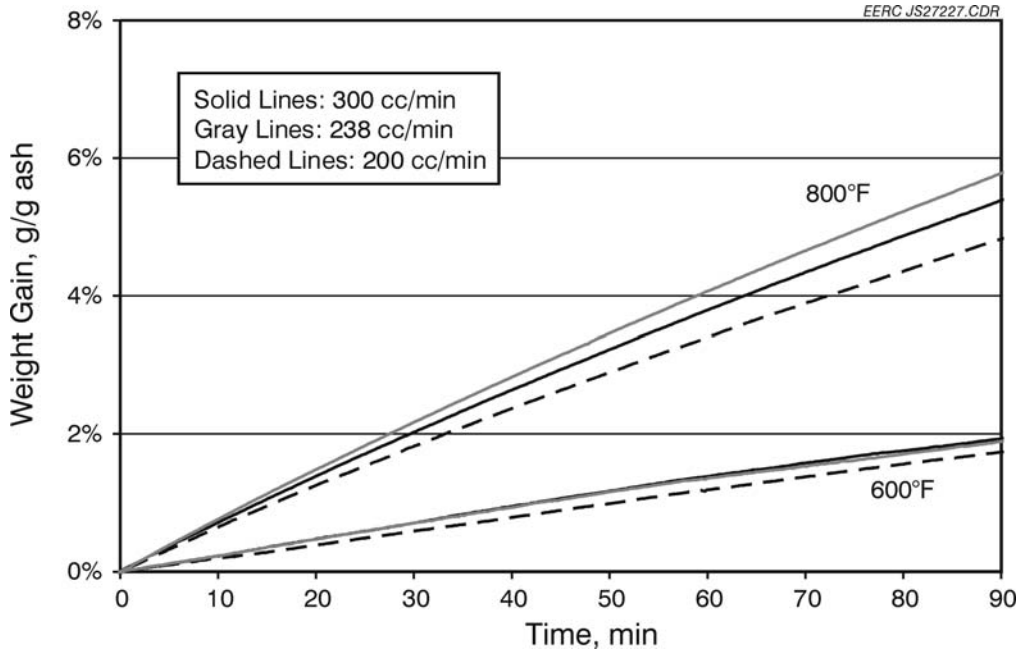

Figure 31. Mass gain in the TGA for 100% cofired ash.

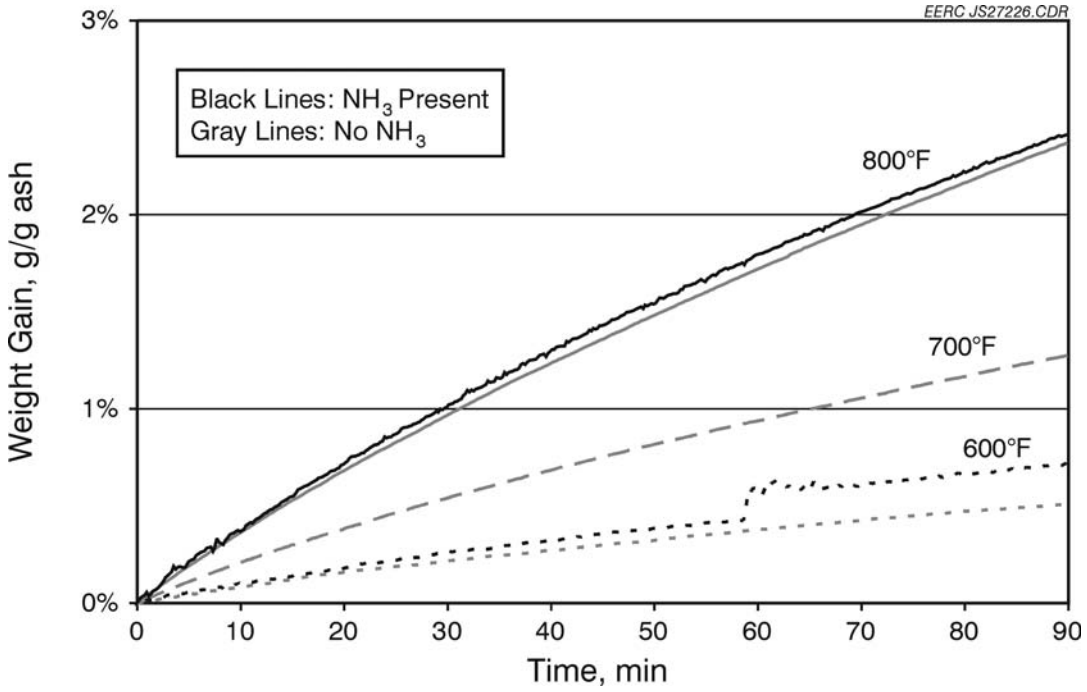

Figure 32. Effect of NH_3 injection on mass gain in TGA. Results depicted are for a 1:1 SCR catalyst-to-ash mixture.

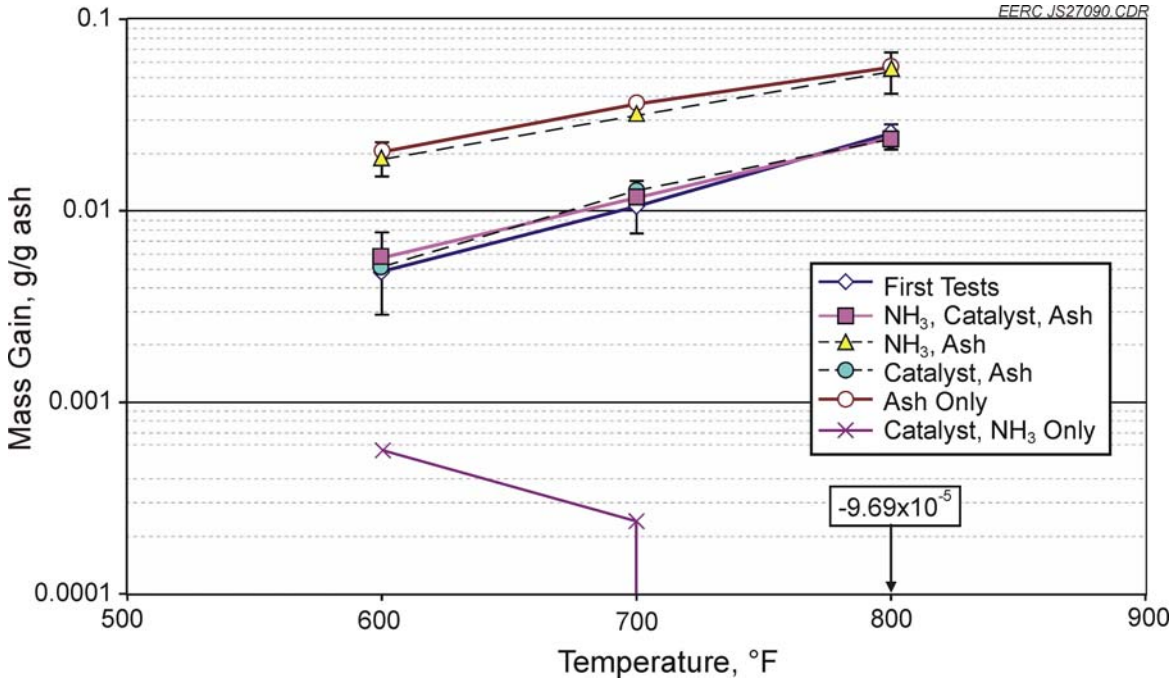

Figure 33. Percent mass gains after 90 minutes for ash, SCR catalyst, and 1:1 (weight) ash–catalyst mixtures under simulated flue gas. Error bars correspond to ±95% confidence intervals using a Student t-distribution.

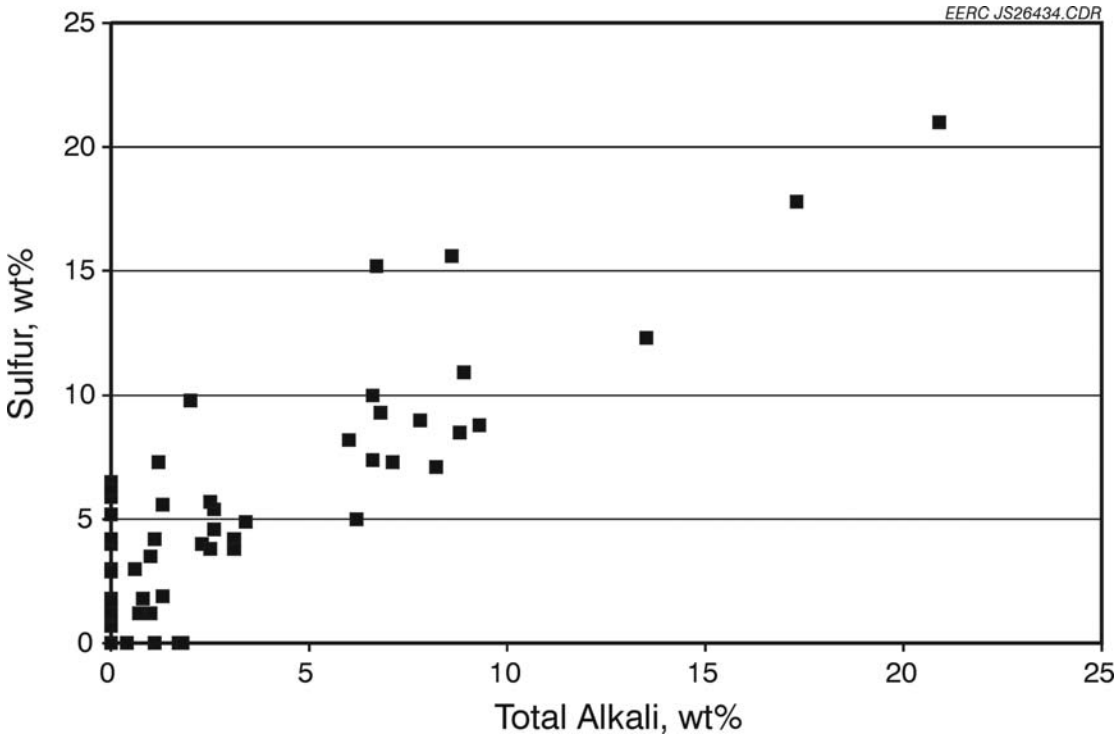

Figure 34. Sulfur content of ash particles as a function of total alkali material.

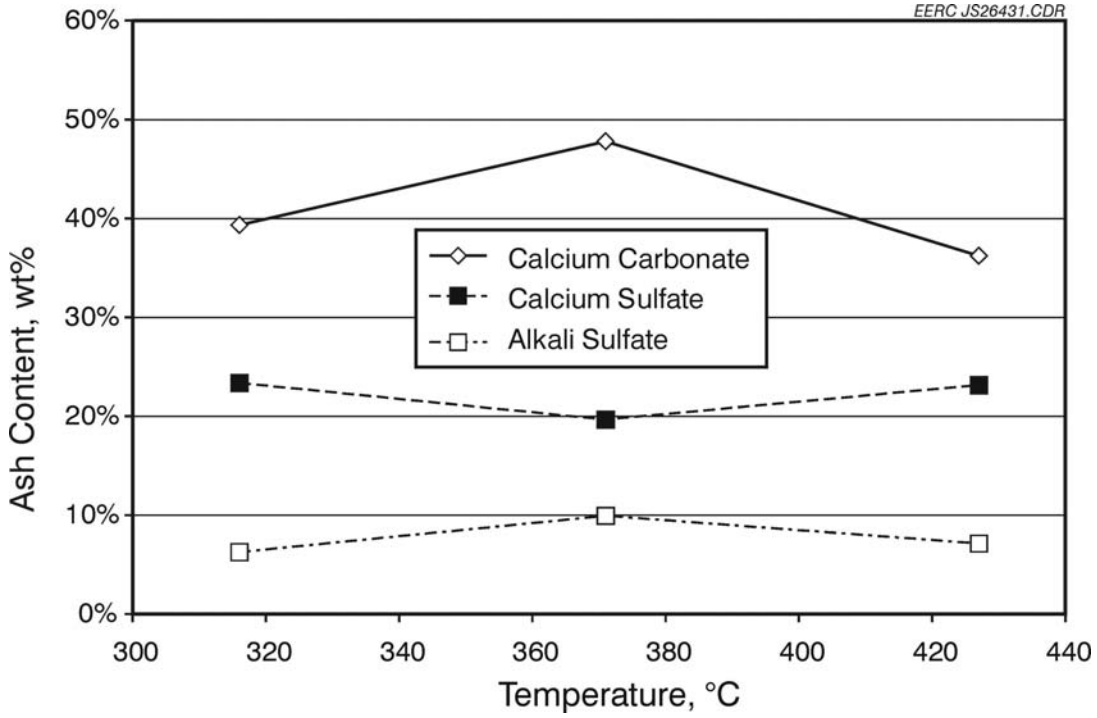

Figure 35. FACT predictions of major carbonate and sulfate speciation at equilibrium.

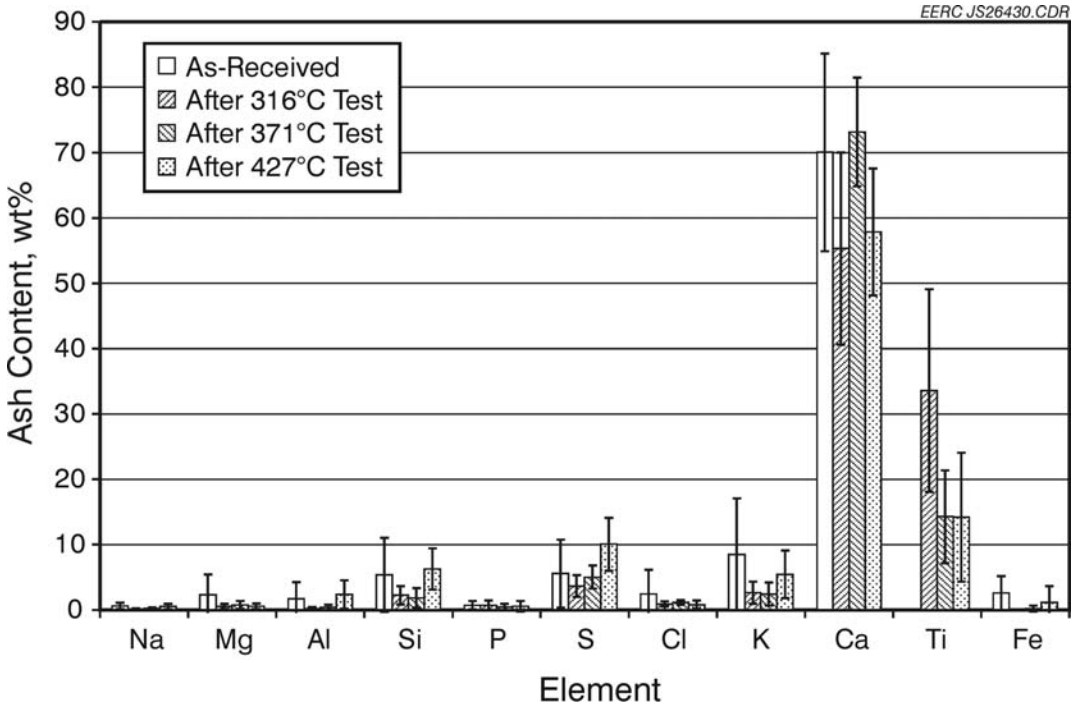

Figure 36. Normalized composition of ash particles analyzed before and after TGA tests. Error bars correspond to 95% confidence intervals.

as-received ash that contained more than 20% sulfur by weight. Ignoring these points gives 2.1±0.9% sulfur in the as-received ash, and using this value to calculate sulfur uptake at each temperature gives results that have an r^2 correlation coefficient of 0.996 with the mass gains in Figure 29.

It is somewhat surprising that sulfur reacted so strongly with alkali material in the TGA, given that thermodynamic modeling predicted that less than 10% total alkali sulfate by weight would form at equilibrium. Sulfur alone constituted 10% of the ash by weight after TGA testing, indicating that more alkali sulfate had formed than thermodynamically allowed. However, thermodynamic modeling considers only equilibrium, not reaction pathways or kinetics. It may be that alkali sulfates were able to form rapidly under TGA conditions but would have further reacted to form more stable species after very long times.

4.5 Modeling Results

The model constructed to predict catalyst activity with time was based on both the TGA data predicting surface activity as a function of time and temperature and on data available from previous tests using the same slipstream reactor used in this work. Figure 38 depicts ash loading with time as predicted by the model and compares with field data for ash loading. As illustrated in Figure 15 and discussed in Section 4.1, the relationship between pressure drop and cross-sectional area is clearly not linear. Ash loading was, therefore, calculated by assuming that the decrease in area over a brief period of time was proportional to the pressure drop through the catalyst. This is somewhat arbitrary, since the pressure drop was fairly constant for most of the

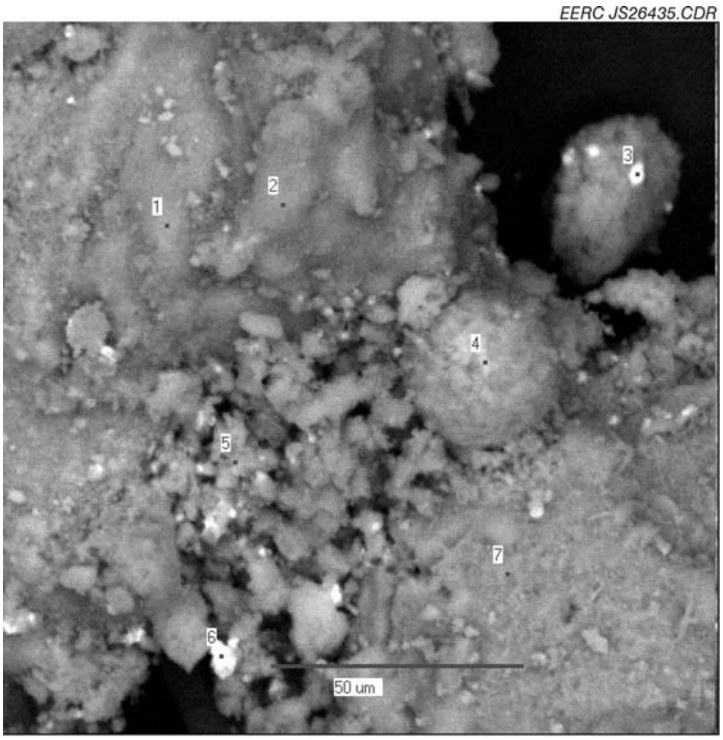

Figure 37. SEM image of ash particles after 600°F TGA test. White spots (e.g., Points 3 and 6) represent titanium dioxide.

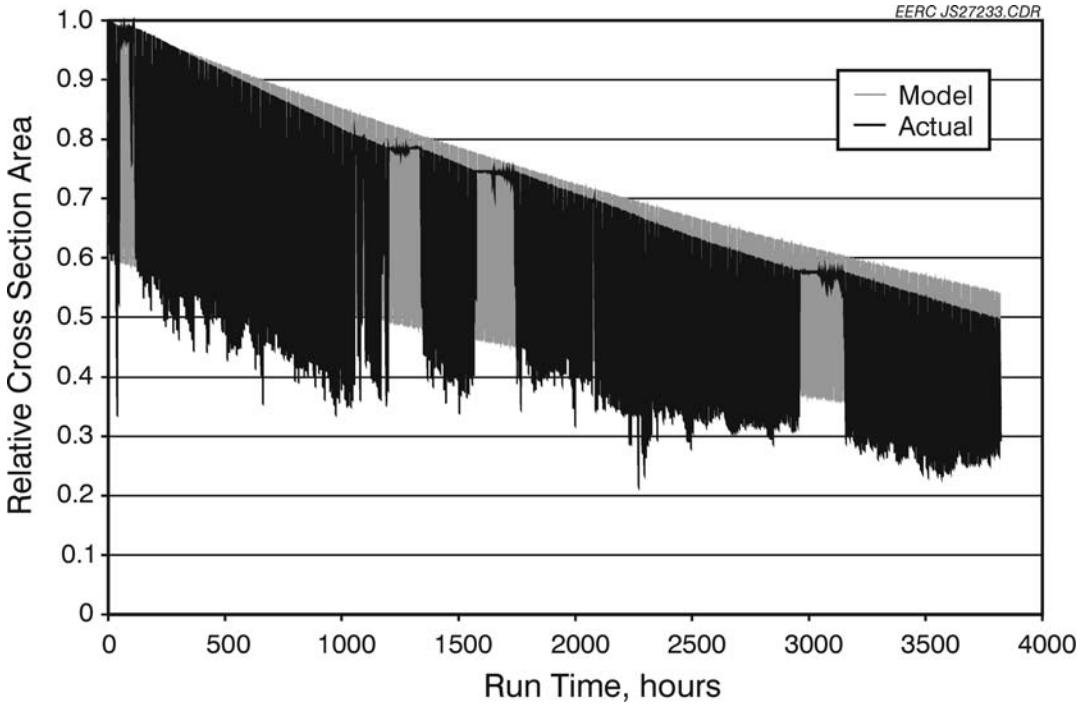

Figure 38. Model predictions and actual ash fouling with time for previous work (100% PRB coal combustion).

test, and there is no theoretical basis correlating fouling rate to pressure drop. However, during the previous work, ash loading could be visually estimated during shutdowns (e.g., half of the catalyst surface might be covered in ash, so ash loading is about 50%). The empirical ash loading matched up fairly well with the trends predicted by assuming a fouling rate proportional to pressure drop.

Figure 39 provides field data over a narrower time range to illustrate the pattern of ash buildup observed in the previous work: Ash would deposit to a certain degree, and then the sootblower would clear away the ash until the reactor was very nearly clean again. Again, the data in Figure 39 are calculated by assuming an arbitrary relationship between rate of change in cross-sectional area and pressure drop, so it may not accurately reflect the true ash loading.

Because of the unexpectedly high ash loading observed in this work, the model results did not correlate to the results observed when cofiring 80% biomass with 20% coal. Any modeling efforts would be particularly difficult in this case because of the somewhat erratic data seen in Figure 15 and because the pulse rate during much of this test was once every 2 minutes as compared with once every 8 hours in the previous work.

Figure 40 provides both model results and field data for catalyst deactivation with time for the previous work. This portion of the model was constructed by extrapolating TGA results. The model does not line up perfectly with the field data, but since the field data contain one point with greater than 100% activity, some error likely lied in the methods used to measure catalyst activity from the recovered sections. Error with the testing method would be observable in Figure 40 because the catalyst did not deactivate by very much, so even an error of a few percent would have a noticeable effect.

Since the model seemed to match fairly well with the field data from the previous work, it was used to estimate catalyst deactivation with time in this work based on the TGA results in Figures 29 and 30. Figure 41 compares the model output with the actual deactivation observed in Figure 22. In this case, the model underpredicted catalyst deactivation. A closer inspection of the model output revealed that no deactivation was predicted to occur until at least 1000 hours had passed. Ignoring this initial plateau provided the adjusted model output seen in Figure 41, which still does not represent the degree of deactivation actually observed.

Although the catalyst sections were actually in place for longer than 43 or 128 days, as discussed in Section 4.1, the extra time in the reactor is insufficient to account for the model inaccuracy. The model predicts that the catalyst would not deactivate to the degree seen after 128 days for about 28,000 hours (1200 days, or 3.25 years). This is approximately twice the length of time that the reactor was in place. Thus the difference between model output and field data observed in Figure 41 is probably due more to deficiencies in the model than to error in interpreting the data.

One reason the model might have underpredicted catalyst deactivation is that deactivation in the field occurred more rapidly or by a different mechanism than observed in the TGA. Since the TGA results were used to generate the model, any difference in conditions between the TGA and slipstream reactor tests would result in modeling error.

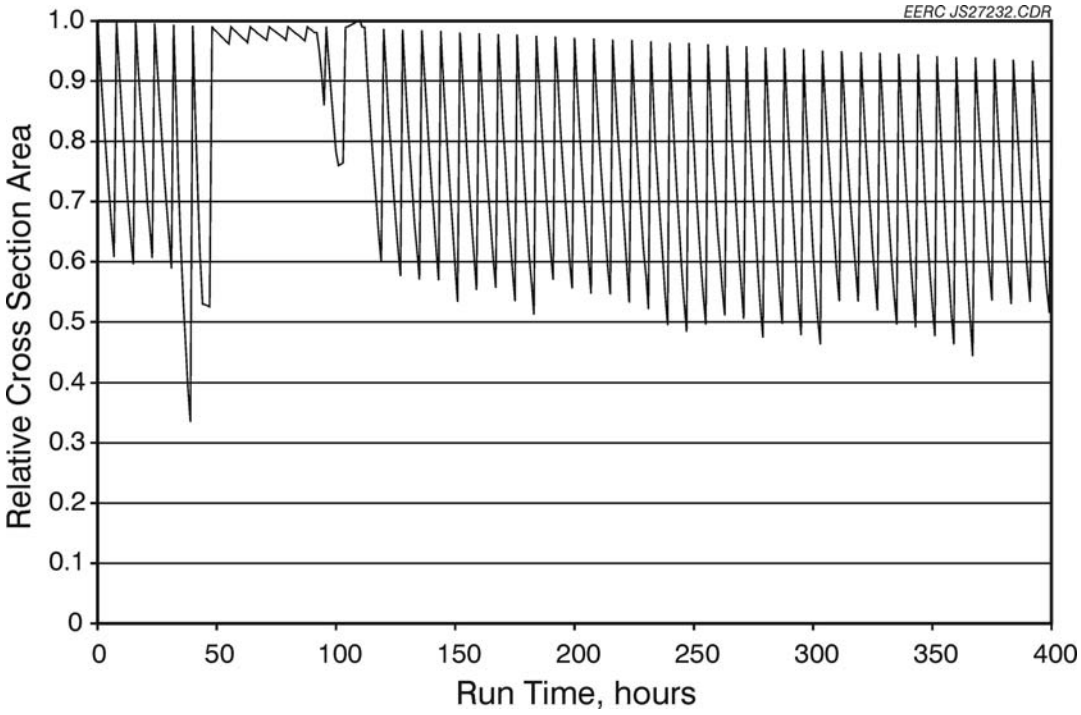

Figure 39. Ash fouling up to 400 hours for 100% PRB coal combustion.

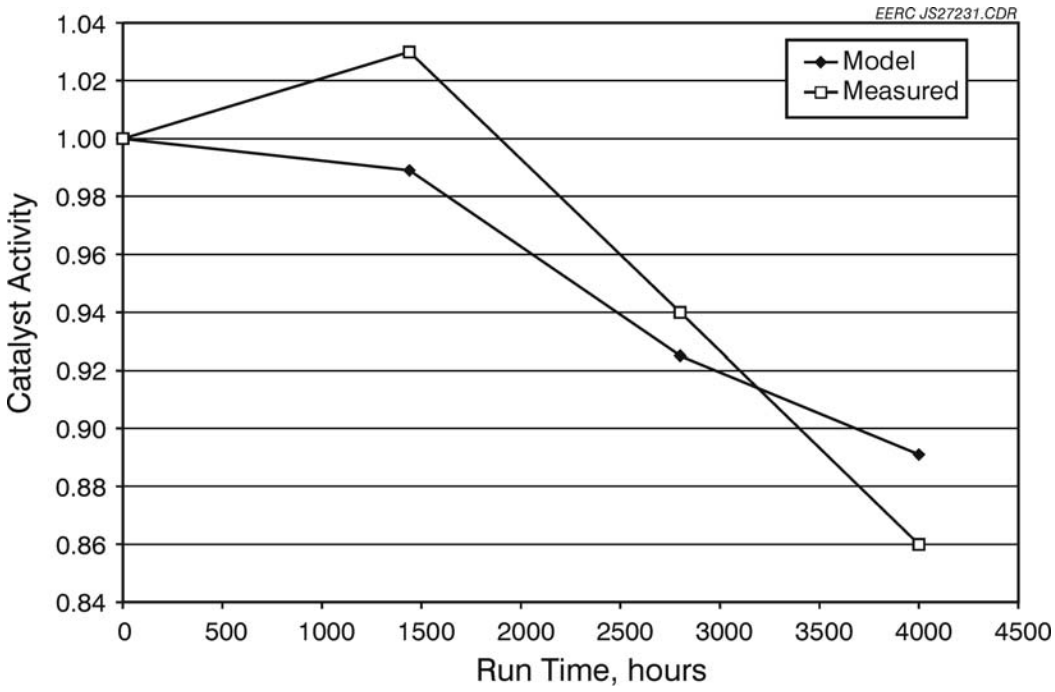

Figure 40. Model predictions and actual catalyst deactivation for previous work (100% PRB coal combustion).

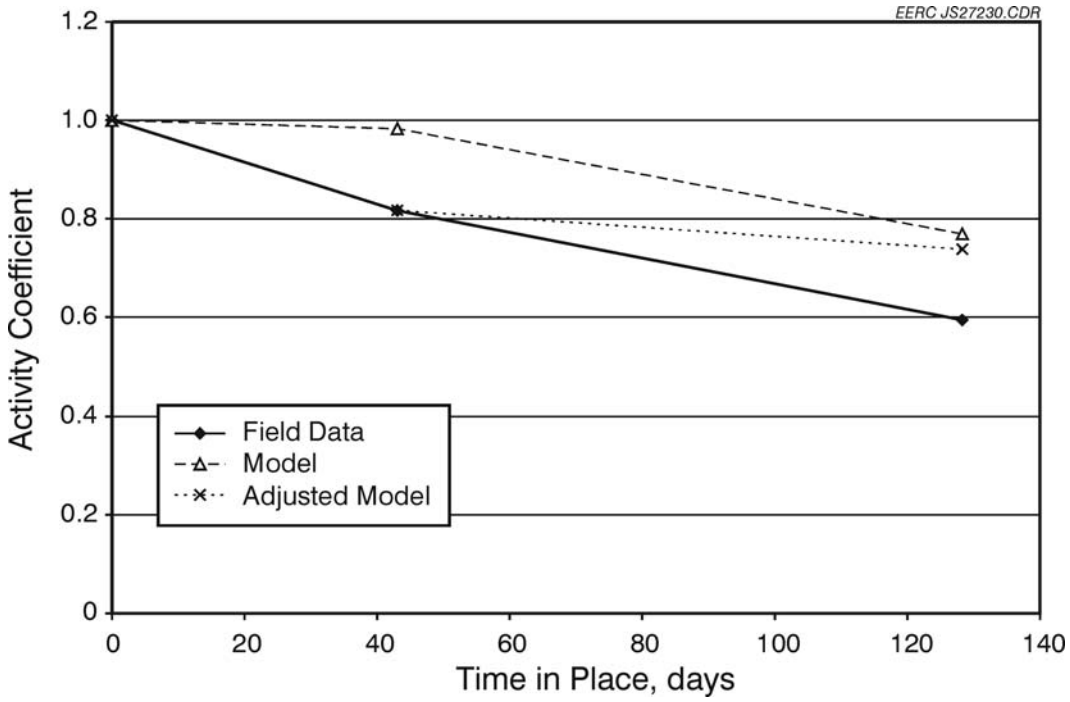

Figure 41. Model predictions and actual catalyst deactivation with time for 80% wood cofired with PRB coal.

One major difference between the TGA work and the field tests is that gas had to pass through a catalyst honeycomb in the field, not simply over and around ground catalyst particles as it did in the TGA. While this does not seem to have affected the model accuracy when predicting catalyst deactivation from the previous work, the match between field data and model results in Figure 40 may be happenstance. A model with a stronger theoretical basis might make better use of the TGA data in predicting deactivation in the field.

5.0 CONCLUSIONS

The SCR slipstream reactor plugged rapidly during this work, even when subjected to frequent sootblowing. This is likely to be a serious problem in other cofiring utilities with high ash loading.

The SCR catalyst deactivated at a very high rate in this test relative to deactivation under coal ash and also relative to deactivation in other tests of cofired biomass and coal. This is a result of the high alkaline-earth content of the hog fuel and of the high ratio of hog fuel to coal, as the alkali and alkaline-earth metals from the biomass formed layers of sulfates where ash deposited near catalyst pores. Since catalyst pores represent the largest fraction of surface area on the catalyst, sulfate growth across pore openings significantly reduced catalyst activity by closure of pore openings.

In this study, the rate of mass gain for ash and catalyst in a simulated flue gas stream was found to be controlled by the ash content only. The rate for catalyst alone is nearly negligible, and when catalyst is mixed at a 1:1 ratio with ash, the rate is only half as great as for pure ash. This is in contrast to previous work that has shown SCR catalyst to be capable of promoting oxidation of SO_2 to SO_3, which in turn led to more rapid mass gain for mixed ash and catalyst (25). As pores represent the regions of greatest catalytic activity, catalytically enhanced sulfation is still a concern for catalyst blinding despite low overall mass gains in the TGA work.

The major mechanism of mass gain in the TGA was alkali sulfate formation via ash alkali reaction with gas-phase sulfur oxides. This was in contrast to previous work that has shown calcium sulfate formation to dominate (25). The difference may be an effect of the higher alkali content of biomass ash or of the high fraction of calcium present as stable calcium carbonate, which may result from firing conditions of the boiler where the ash was obtained.

Because of the typically higher-than-coal levels of alkali and alkaline-earth elements present in biomass fuels that are available for sulfation at typical SCR temperatures, the use of SCR technology and biomass cofiring needs to be carefully evaluated prior to implementation.

6.0 REFERENCES

1. *Annual Energy Review: 2003*; Report No. DOE/EIA-0384(2003); U.S. Department of Energy, Energy Information Administration, U.S. Government Printing Office: Washington, DC, 2004.

2. Robinson, A.L.; Rhodes, J.S.; Keith, D.W. Assessment of Potential Carbon Dioxide Reductions Due to Biomass–Coal Cofiring in the United States. *Environ. Sci. Technol.* **2003**, *37* (22), 5081–5089.

3. Liu, D.C.; Mi, T.; Shen, B.X.; Feng, B. Reducing N_2O Emissions by Cocombustion of Coal and Biomass. *Energy Fuels* **2002**, *16* (2), 525–526.
4. Wieck-Hansen, K.; Overgaard, P.; Larsen, O.H. Cofiring Coal and Straw in a 150-MW_e Power Boiler Experiences. *Biomass Bioenergy* **2000**, *19*, 395–409.

5. Beck, J.; Brandenstein, J.; Unterberger, S.; Hein, K.R.G. Effects of Sewage Sludge and Bone Meal Cocombustion on SCR Catalysts. *Appl. Catal. B: Environ.* **2004**, *49*, 15–25.

6. Baxter, L.; Koppejan, J. Biomass–Coal Cocombustion: Opportunity for Affordable Renewable Energy. *EuroHeat Power* **2004**, *1*.

7. *NO_x Budget Trading Program: 2003 Progress and Compliance Report*; EPA-430-R-04-010; U.S. Environmental Protection Agency, Office of Air and Radiation, Clean Air Market Programs: Washington, DC, 2004.

8. McAdams, J.D.; Reed, S.D.; Itse, D.C. Minimize NO_x Emissions Cost-Effectively. *Hydrocarbon Process.* **2001**, *6*, 51–57.

9. Hartenstein, H.U.; Gutberlet, H.; Licata, A. Utility Experience with SCR in Germany. In *Proceedings of the 16th Annual International Pittsburgh Coal Conference*; Pittsburgh, PA, Oct 11–15, 1999.

10. Buecker, B. SCR Design. *Power Eng.* **2002**, *Aug*, 24–28.

11. *Demonstration of Selective Catalytic Reduction Technology for the Control of NO_x Emissions from High-Sulfur-Coal-Fired Boilers*. www.netl.doe.gov/path: cctc/summaries/scr/images/scr_schematic.jpg (accessed June 2005).

12. Benson, S.A.; Hurley, J.P.; Zygarlicke, C.J.; Steadman, E.N.; Erickson, T.A. Predicting Ash Behavior in Utility Boilers. *Energy Fuels* **1993**, *7*, 746–754.

13. Kamata, H.; Takahashi, K.; Ingemar Odenbrand, C.U. The Role of K_2O in the Selective Reduction of NO with NH_3 Over a $V_2O_5(WO_3)/TiO_2$ Commercial Selective Catalytic Reduction Catalyst. *J. of Molec. Catal. A: Chem.* **1999**, *139* (2–3), 189–198.

14. Wiltsee, G.A. Biomass Combustion Technologies for Power Generation. In *Proceedings of the 1st Biomass Conference of the Americas: Energy, Environment, Agriculture, and Industry, Vol. 1*; Burlington, VT, Aug 30 – Sept 2, 1993.

15. Franklin, H.N. Hitachi. Personal communication, 2002.

16. Wieck-Hansen, K. Cofiring Coal and Straw in PF Boilers – Performance Impact of Straw with Emphasis on SCR Catalyst for deNO_x Catalysts. In *Proceedings of the 16th Annual International Pittsburgh Coal Conference*; Pittsburgh, PA, Oct 11–15, 1999.

17. Khodayari, R.; Ingemar Odenbrand, C.U. Regeneration of Commercial TiO_2–V_2O_5–WO_3 SCR Catalysts Used in Bio Fuel Plants. *Appl. Catal. B: Environ.* **2001**, *30* (4), 87–99.

18. *Biomass Combustion and Cofiring: An Overview*; IEA Bioenergy, International Energy Agency.

19. IEA Task 32: Biomass Database. www.ieabcc.nldatabase/biomass.php (accessed June 2005)

20. *Compilation of Air Pollutant Emission Factors, Volume 1: Stationary Point and Area Sources—AP 42, 5th ed.*; U.S. Environmental Protection Agency, Emissions Factors & Policy Applications Center. www.epa.gov/ ttn/chief/ap42; Section 1.7. (accessed June 2005).

21. Benson, S.A.; Hurley, J.P.; Zygarlicke, C.J. Studies on Calcium-Based Deposition in Utility Boilers. In *Proceedings of the Conference on Effects of Coal Quality on Power Plants*; St. Louis, MO, Sept 1990.

22. Zygarlicke, C.J.; Steadman, E.N. Advanced SEM Techniques to Characterize Coal Minerals. *Scan. Microsc.* **1990**, *4* (3), 579–590.

23. Galbreath, K.; Zygarlicke, C.; Casuccio, G.; Moore, T.; Gottlieb, P.; Agron-Olshina, N.; Huffman, G.; Shah, A.; Yang, N.; Vleeskens, J.; Hamburg, G. Collaborative Study of Quantitative Coal Mineral Analysis Using Computer-Controlled Scanning Electron Microscopy. *Fuel* **1996**, *75* (4), 424–430.

24. Fogler, H.S. *Elements of Chemical Engineering Reaction Design*, 3rd ed.; Prentice Hall: Upper Saddle River, NJ, 2002.

25. Laumb, J.D.; Benson, S.A.; Crocker, C.R.; Gunderson, J.R.; Jensen, R.R. *JV 31 – Evaluation of Potential SCR Catalyst Blinding During Coal Combustion and Add-On: Impact of SCR Catalyst on Mercury Oxidation in Lignite-Fired Combustion Systems*; Final Report for U.S. Department of Energy Cooperative Agreement No. DE-FC26-98FT40321; Energy & Environmental Research Center, Grand Forks, ND, Nov 2004.

26. Cichanovicz, J.E.; Muzio, J. Twenty-Five Years of SCR Evolution: Implications for U.S. Applications and Operation. EPRI–DOE–EPA Combined Utility Air Pollution Control Symposium: The MEGA Symposium, AWMA, Chicago, IL, Aug 20–23, 2001.

27. Svachula, J.; Alemany, L.J.; Ferlazzo, N.; Forzatti, P.; Tronconi, E. Oxidation of SO_2 to SO_3 over Honeycomb DeNoxing Catalysts. *Ind. Eng. Chem. Res.* **1993**, *32*, 826–834.

28. Dollimore, D. The Thermal Decomposition of Oxalates, a Review. *Thermochim. Acta* **1987**, *117*, 331–363.

29. Hurley, J.P.; Benson, S.A.; Erickson, T.A.; Allan, S.E.; Bleber, J. *Project Calcium*; Topical Report for U.S. Department of Energy Cooperative Agreement No. DE-FC21-86MC10637; Energy & Environmental Research Center, Grand Forks, ND, Sept 1992.